Sequential and dynamic coding of water-sucrose categorization in rat gustatory cortices

Germán Mendoza[1], Esmeralda Fonseca[2,3], Hugo Merchant[1], Ranier Gutierrez[3,4*]

1 Laboratory of Systems Neurophysiology, Institute of Neurobiology, National Autonomous University of Mexico, Juriquilla Querétaro, 76230, Mexico.

2 Princeton Neuroscience Institute, Princeton University, Princeton, New Jersey, 08544, United States.

3 Laboratory of Neurobiology of Appetite, Department of Pharmacology, Center for Research and Advanced Studies of the National Polytechnic Institute, Mexico City, 07360, Mexico.

4 Centro de Investigación Sobre el Envejecimiento CIE Cinvestav sede Sur.

*Correspondence: ranier@cinvestav.mx

Summary

The gustatory system underlies our conscious perception of sweetness and allows us to distinguish a sweet solution from plain water. However, the neural mechanisms in gustatory cortices that enable rats to differentiate sweetness from water remain elusive. In this study, we designed a novel sucrose categorization task in which rats classified water from a gradient of sucrose solutions. We found that in the anterior Insular Cortex (aIC) and the Orbitofrontal Cortex (OFC), neural activity prioritized encoding the categorization of water versus sucrose rather than the specific concentrations within the sucrose solutions. aIC neurons more rapidly encoded sucrose/water distinction, followed by the OFC. In contrast, the OFC encoded choice information slightly earlier than aIC, but both gustatory cortices maintained a comparable encoding of the rat's choices in parallel. The encoding of sensory and categorical decisions was dynamic and sequentially encoded, forming a sequence of encoding neurons spanning the entire length of a task trial. Our results demonstrate that sucrose categorization relies on dynamic encoding sequences in the neuronal activity of aIC and the OFC rather than static, long-lasting (sustained) neural representations. Single-cell, population decoding, and principal component analyses confirmed our results. This aligns with the concept of a dynamic code, where the brain updates its representation of sucrose categorization as new information becomes available. Additionally, aIC and the OFC rapidly encoded reward outcomes. Our data supports the view that gustatory cortices use sequential and dynamic coding to compute sensorimotor transformations from taste detection to encoding categorical taste decisions and reward outcomes.

Keywords

Sucrose, taste categorization, perceptual decision-making, gustatory cortices, firing rate encoding, dynamic coding

Introduction

Sucrose, a disaccharide commonly found in table sugar and fruits, is a sweet-tasting, high-calorie carbohydrate that most animals find palatable. Sucrose also induces the conscious experience of sweetness in humans and likely rodents as well. However, excessive consumption can contribute to obesity and heighten the risk of various obesity-related chronic diseases, including type 2 diabetes, heart disease, and stroke (Gutierrez et al., 2020). Despite its great importance, how rats know that a solution contains sucrose or pure water and how the brain represents and assigns information about sucrose, regardless of its concentration, into the sucrose category, distinguishing it from water is not yet known. Much research has been devoted to understanding how the nervous system detects and processes the sweet compounds at the periphery. For example, the sweet (T1R2/T1R3) taste receptor has been identified (Nelson et al., 2001), and geniculate ganglion sensory cells have been characterized (Barretto et al., 2015; Wu et al., 2015). However, how the brain represents sweet taste information, particularly gustatory cortices, is less well-understood. The anterior insular cortex (aIC) and the orbitofrontal cortex (OFC) play a crucial role in gustation as primary and secondary taste cortices, respectively (Rolls et al., 1990). These regions evaluate the taste and value of food (Rolls, 2023), including its sweetness (Fonseca et al., 2018; Kogan and Fontanini, 2024). Regarding cortical taste processing, most experiments have focused on passive processing by a part of the insular cortex that contains the Gustatory Cortex (GC) (Vincis and Fontanini, 2019), i.e., in anesthetized or passive awake subjects that were only required to lick to receive delivery of tastants (Maier and Katz, 2013; Rolls et al., 1990; Scott et al., 1991; Stapleton et al., 2006; Thorpe et al., 1983) and few studies were interested in how the brain uses the gustatory percepts to make decisions actively (Fonseca et al., 2018; Gutierrez et al., 2010; Lang et al., 2023; Vincis et al., 2020). We previously investigated the activity in aIC and OFC of rats performing discrimination tasks with varying sucrose concentrations (Fonseca et al., 2018). We reported that neurons in these regions encode sweetness intensity, choice behavior, and reward outcomes during a task where rats discriminated between "low" (3% sucrose) and "high" (18% sucrose) solutions (Fonseca et al., 2018). These neurons encoded multiple aspects of the task, including stimulus intensity, the subjective perception of sweetness, the direction of motor responses, and the delivery and omission of rewards. However, one key question remains unanswered: how precisely do these gustatory cortices represent the gradations of sucrose intensity? In other words, in a categorization task, can the neural activity distinguish between different sucrose concentrations with high fidelity? Previous studies, including ours, have suggested that some neurons in the gustatory cortices exhibited activity that is monotonically related to the concentrations of sweet tastants (Fonseca et al., 2018; Maier and Katz, 2013; Rolls et al., 1990; Scott et al., 1991; Stapleton et al., 2006; Thorpe et al., 1983). Except for a few studies (Fonseca et al., 2018; Kogan and Fontanini, 2024), the importance of these parametric neural representations for behavior has not been quantified. In addition, the temporal

encoding patterns of single neurons in the gustatory cortices have not been described in an active context of decision-making or how these patterns are reflected in low-dimensional representations of population activity.

To address these questions, we employed single-neuron, neural population decoding, and dimensionality reduction techniques to compare the encoding dynamics in aIC and the OFC during a sucrose categorization task. In this task, after sampling one drop of water-based liquid, rats were required to report whether the liquid stimulus was plain water or whether they perceived sucrose; sucrose could be delivered in one out of five different concentrations, ranging from 0.5 to 20%. We found that the distinction between the identity/quality of the tastant, water versus sucrose, but not sucrose's intensity (i.e., specific concentrations), was the most robust stimulus feature-related information in the population activity of aIC and OFC neurons. We also found that neurons in both cortices encoded the stimulus-related information and the rat's choices dynamically, with significant information carried by different neurons at different time points, resulting in reproducible encoding sequences. In addition, some neurons switched their encoding pattern from one perceptual decision or outcome to another, or from one task variable to another. Finally, we found that all the main features observed in the activity of single neurons or with population decoding techniques were also reflected in a linear low-dimensional state space of neuronal population activity.

Behavioral Results

Rats could solve the sucrose-categorization task

Eleven male Sprague-Dawley rats were trained in a novel sucrose categorization task. The task involved classifying between water and various sucrose concentrations. The trial structure was as follows: rats started each trial by licking a central spout (2-3 times) to receive a 10 μL water or sucrose solution (Stimulus delivery epoch). Following the licks in the central stimulus spout, rats chose a lateral response spout (Water or Sucrose-associated spouts) and emitted one dry lick (Response epoch). A correct choice triggered the delivery of three water drops as a reward, one per each subsequent lick; an incorrect choice resulted in no reward. During each trial, one of six stimuli was delivered: water (0% Sucrose) or sucrose (0.5, 1.3, 3.2, 7.9, and 20% w/v). Water-stimulus trials comprised 50% of the trials in each session, with the remaining sucrose concentrations equally distributed.

We plotted the average psychometric performance to demonstrate that rats could categorize water from sucrose, regardless of concentration (**Figure 1B**). The graph depicts the probability of rats associating the Stimulus with a "Sucrose-Response"

plotted against the varying sucrose concentrations. As expected, the probability of a “Sucrose-Response” increased steadily with higher sucrose concentrations. The absolute threshold, defined as the concentration at which rats responded to the "Sucrose spout" in 50% of the trials, was determined to be 0.35% w/v. The probability of responding to the "Sucrose spout" for 0.5 and 1.3% concentrations was near the chance of 50%, indicating that these concentrations were the hardest to detect. Thus, rats could not reliably distinguish these two concentrations from water. The presentation of Water- and Sucrose-Stimulus trials was balanced; however, rats made a significantly higher proportion of Water- compared to Sucrose-Responses (0.518 ± 0.081 vs. 0.481 ± 0.081, respectively; t-test, $t_{(200)} = 3.24$, $p < 0.01$; **Figure 1C)**. The proportion of correct/rewarded trials was also slightly higher for Water- compared to Sucrose-Response trials (0.385 ± 0.052 vs. 0.366 ± 0.043; t-test, $t_{(200)} = 2.80$, $p < 0.01$, **Figure 1C**). Altogether, these results suggest that the increased proportion of Water-Response trials is because of the difficulty of correctly categorizing the lowest sucrose concentrations, 0.5 and 1.3%.

Sucrose palatability was reflected as additional licking in the Stimulus spout

Once the tastant is delivered, the time spent licking the Stimulus spout is a measurement that reflects the palatability or hedonic value of the gustatory cue (Perez et al., 2013). In our categorization task, the Stimulus-spout licking duration increased as a function of sucrose concentration; this response pattern was maintained during correct trials ($F_{(5, 600)} = 59.34$, $p < 0.001$; Tukey-Kramer critical value) and incorrect trials ($F_{(5, 573)} = 48.21$, $p < 0.001$) (**Figure 1D**). Thus, despite the trial’s outcome, there is still a preserved palatability effect throughout Stimulus-spout licking: That is, licking time increases for higher palatable stimuli. However, licking in the Stimulus spout for the same sucrose concentration also varies depending on the subject’s performance (error vs. correct trials). We observed that the easiest-to-detect (0 and 20%) and the most difficult-to-detect (0.5 and 1.3%) concentrations significantly differed in licking durations (For statistics, see **Supplementary Table 1; Figure 1D**), with the easiest (0 and 20%) exhibiting longer, and the most difficult (0.5 and 1.3%) shorter licking durations in error compared to correct trials (**Figure 1D**). Interestingly, longer lick durations during "easiest-to-detect" stimulus trials (0 and 20%), where rats failed categorization, suggest they might not have fully detected the stimuli. Conversely, shorter lick durations for the two low sucrose concentrations (0.5 and 1.3%), often miscategorized as “water,” contradict the expected pattern. These shorter lick durations, similar to correctly categorized Water trials, suggest the licking response might be influenced by the subject's perception of the taste, not just pure palatability. Therefore, it's possible that subjects perceived the 0.5% and 1.3% sucrose as “water,” leading to a lower palatability oromotor reflex – reflected by the shorter licking durations on those trials. Overall, these results suggest that, in taste-guided decisions, the duration of dry licks emitted after stimulus sampling might reflect the palatability and the subject’s perception.

Movement time, during correctly categorized trials, did not contain information about palatability

Interestingly, rats exhibited similar movement times (time between the last lick in the Stimulus spout and the first lick in the Response spout) across all stimuli during correct responses ($F_{(5, 600)} = 1.83$, $p = 0.104$; **Figure 1E**). In agreement with other taste psychophysical tasks (Perez et al., 2013). Thus, it suggests that the movement time was ballistic and confident in correct trials and did not reflect taste palatability. However, during error trials, movement times significantly increased for Water- and the highest Sucrose-Stimulus concentration trials ($F_{(5, 573)} = 7.62$, $p < 0.001$; **Figure 1E**). This suggests that rats hesitated longer during incorrect choices, particularly for high sucrose concentrations. It is important to note that during movement from the central to lateral spout, the animals keep updating their choices, and thus, this epoch is rich in decision-making information.

Rats rapidly detect reward delivery from omission

For correct trials, rats exhibited sustained licking following reward delivery (3 drops of water as a reward): they spent significantly more time licking the Response spout after rewarded trials compared to non-rewarded ones (correct: 0.85 ± 0.137 s vs. incorrect: 0.32 ± 0.146 s; mean ± SD; $t_{(1183)} = 65.3$, $p < 0.001$, **Figure 1F**). These findings suggest that rats not only distinguished a reward but also rapidly stopped licking when no reward was delivered (error trial), which allows rats to rapidly re-start another trial, complete more trials, and thus collect more rewards throughout the session; the latter, confirms the ability of rats to adapt their behavior based on reward outcomes swiftly.

Electrophysiological results

A single drop of tastant triggers a brain-wave activity pattern

We recorded 400 neurons from the anterior Insular Cortex (aIC) and 449 neurons from the Orbitofrontal Cortex (OFC) in the left hemisphere of rats performing the sucrose categorization task. To investigate the temporal dynamics of task-information encoding, we conducted analyses based on signal detection theory on the Firing Rates (FRs) of each neuron per trial during 100-ms time windows (Fonseca et al., 2018; Samuelsen and Fontanini, 2017; Vincis et al., 2020) with moving steps of 10-ms (Lara et al., 2009). We found similar proportions of neurons encoding the Stimulus, the Choice, and the Outcome in aIC and the OFC. In both gustatory cortices, the Stimulus was the less represented variable, with 11.6 and

14.22% of the Stimulus-encoding neurons in the aIC and the OFC, respectively (z = -1.109, p = 0.267); followed by the Choice-encoding subset, with 30.15 and 34.36% cells (z = -1.278, p = 0.200); and finally, the Outcome-encoding subset with 54.12 and 54.74% of neurons in aIC and OFC, respectively (z = -1.175, p = 0.857). Thus, a single drop of taste stimulus triggered a brain-wave activity that gradually recruited more and more cortical neurons, from Stimulus delivery up to the reward Outcome, encompassing all relevant task-variables that may give rise to trial structure representation (Fonseca et al., 2018; Laboratory et al., 2023). Furthermore, we found relatively small neuronal sub-populations that encoded more than one variable (**Figure 2 Supplementary 1**). In the following paragraphs, we describe these results in detail.

Neurons in aIC and OFC encoded the categorical distinction between water and sucrose

To identify neurons that encoded Stimulus information in a categorical manner, we assessed differences in the neural activity during Water- (Sucrose 0%) against Sucrose-Stimulus (Sucrose 0.5, 1.3, 3.2, 7.9, 20%) trials, for each single neuron recorded. Only correct trials were included in the analysis. For each cell, FR distributions for Water- and Sucrose-Stimulus trials were calculated per time-bin. The distribution overlap was measured by computing the area under the Receiver Operating Characteristic (auROC) curve, referred to as Stimulus-auROC. The auROC curve values range between 0 and 1; values closer to the edges, 0 or 1, indicate fully segregated distributions, while a 0.5 value indicates complete overlap. It is important to note that, in categorization tasks, there is a trial-by-trial correlation between the Stimulus and the subject's Choice during correct trials, making it challenging to dissociate neural activity associated with the Stimulus from the Choice/Response. We addressed this problem by computing an additional auROC curve that takes into account not the Stimulus received (Water or Sucrose) but what the subject perceived according to their Choice/Response; this curve will be referred to as the “Choice Probability index.” We considered Stimulus-encoding when statistically significant Stimulus-auROC time-bins were also higher than the corresponding Choice Probability index. Neurons with five or more consecutive time bins fulfilling these criteria were classified as Stimulus-encoding cells. The window containing the largest significant auROC values was considered the best Categorical Stimulus-encoding time-window. Furthermore, we determined the Stimulus-encoding cells' best time-window for positively or negatively monotonic changes as a function of Stimulus concentration: increasing or decreasing FRs with higher concentrations. The time window with the largest significant Pearson correlation r-value was selected as the best time-window for Intensity Stimulus-encoding.

We found a small group of categorical/quantal Stimulus-encoding cells (Water vs. Sucrose) in both aIC (45 out of 388, 11.6%) and OFC (60 out of 422, 14.22%). The percentage of Stimulus-encoding neurons in each cortex was not significantly different ($z = -1.109$, $p = 0.267$), in agreement with previous findings that suggest that taste coding is sparse and distributed (Chen et al., 2020; Fonseca et al., 2018). **Figure 2A** shows examples of aIC and OFC Stimulus-encoding neurons. The aIC neuron showed phasic categorical Stimulus-selective activity around 50 ms after tastant delivery; it rapidly responds to Water-Stimulus and exhibits a transient inhibition after Sucrose-Stimulus delivery. In contrast, the OFC neuron rapidly ramped up (around 50 ms) but exhibited Stimulus-selective activity after 200 ms from Stimulus delivery, with a higher FR during Sucrose- compared to Water-Stimulus trials. The time intervals containing the more significant neural activity difference between Water- and Sucrose-Stimulus trials, which is the best time-window for categorical Stimulus-encoding (see cyan asterisks over the time axis, **Figure 2A**), occur at different moments after Stimulus delivery. Furthermore, both cells also significantly encoded the Intensity (all concentrations) of the Stimulus with different temporal signatures, as shown by the cyan-shaded rectangle signaling the best time-window of Intensity Stimulus-encoding (**Figure 2A**). The mean activity elicited by each stimulus concentration during this best time-window is shown in **Figure 2B**: The aIC and OFC cells showed a decrease and increase in FR as a function of concentration (left and right panels, respectively). Cells with negative and positive monotonic changes relative to sucrose concentration were found in both taste cortices; out of the 45 aIC Stimulus-encoding neurons, 18 exhibited a positive relationship, and 27 had a negative relationship between FR and stimulus concentration. From 60 Stimulus-encoding OFC neurons, 27 and 33 showed positive and negative correlations, respectively (**Figure 2C**). The presence of more neurons with a negative than positive correlation substantiates that water is, *per se*, a taste stimulus that strongly drives the activity of gustatory cortices (de Araujo et al., 2003; Gutierrez et al., 2010; MacDonald et al., 2009; Rosen et al., 2010).

Transient sequences of Stimulus-encoding neurons in the aIC and OFC reliably represent the distinction between sucrose and water

The time-windows for Categorical- (Water vs. Sucrose) and Intensity- (all six concentrations) Stimulus-encoding occurred at different trial points as moving bumps. We wondered whether the encoding information of each cell would sequentially encompass the entire Stimulus epoch. To visualize the sequential encoding of each cell belonging to the Stimulus-encoding subset, we plotted the color-coded auROC values across the Stimulus epoch from -250 ms to +800 ms aligned to Stimulus delivery (**Figure 2C**). Neurons were sorted based on their auROC peak latency. Note that the information encoding pattern in both areas is dynamic, i.e., each neuron exhibited higher auROC values during short window times, and the encoding windows of different cells are scattered across time.

Accordingly, the Stimulus-encoding peak time does not occur simultaneously across cells but is distributed after the Stimulus delivery. To compare the sequential encoding of the neural populations in aIC and the OFC, we adapted the Sequentiality Index (SqI) developed by (Zhou et al., 2020). The original index is computed on the FRs of the neural populations and is bounded between 0 and 1. The SqI approaches 1 when the peak times of each neuron homogeneously tile the entire duration of interest, and one neuron is active at every moment in time, with the temporal fields being non-overlapping and approaching 0 otherwise. The index is computed from the Peak Entropy (PE), which measures the entropy of the distribution of peak times across the entire neural population, and Temporal Sparsity (TS), which measures the entropy of the distribution of normalized activity in any bin. Here, we applied the SqI to the auROC values shown in **Figure 2C** (see Methods). This analysis examines the sequential nature of information encoding in aIC and the OFC. Used in this way, PE reflects how homogeneously the encoding periods of the different neurons tile the entire analyzed period, with values close to one for more homogenous covering and zero otherwise, and TS measures how much of the activity at each point in time can be attributed to a single neuron, with values of zero and one corresponding to overlapped and not-overlapped encoding periods, respectively. We found that Stimulus was encoded in sequence for both cortical regions, but it was slightly more sequential in aIC (SqI: 0.749; PE: 0.981; TS: 0.571) than in the OFC (SqI: 0.695; PE: 0.939; TS: 0.515). Also, the relatively high SqI depended mainly on the PE, not on the TS, indicating that the encoding periods homogeneously covered the analyzed Stimulus-epoch but with a middle-overlapping of the encoding periods of the different cortical neurons.

To test whether the sequences of neural encoding are reproducible and not a random product, we compared them in different subsets of trials. First, auROC values were obtained from two randomly partitioned sets of trials. This resulted in two matrices of auROC values per cortical area. Next, for each cortical area, we sorted the cells in matrix one by their latencies to peak auROC, used the same indexes to sort the second matrix, and computed the Mean-Squared Error (MSE) between the two sorted matrices to measure pattern similarity. For aIC and OFC neurons, the MSE between splits was 0.0036 and 0.0021, respectively. A permutation test showed that these relatively low errors in the aIC and the OFC populations could not be obtained by chance ($p < 0.001$), supporting that Stimulus-encoding sequences are highly reproducible.

Another main observation in the color-coded maps of **Figure 2C** is that the encoding of Stimulus information by OFC neurons is delayed, about 200 ms, compared to that of aIC neurons. This can be appreciated in **Figure 2D**, in which the average auROC across statistically significant neurons is shown for both cortical areas. The mean auROC of the aIC population tends to increase rapidly (> 50 ms) and steadily after the Stimulus delivery. In contrast, the Stimulus selectivity for the OFC remained low until 300 ms, when it abruptly increased, outperforming aIC. **Figure 2E** shows the

cumulative distributions of the proportion of neurons that reached their peak auROC values across time bins. The rapid neuronal recruitment in the aIC followed by the OFC can be seen. A two-sample Kolmogorov-Smirnov test on the time bins at which the neurons of aIC and OFC reached their peak auROC values ($p < 0.001$) supports this observation. These results unveiled that Stimulus-encoding aIC cells were recruited first, followed by the OFC Stimulus-encoding subset.

Neural activity in aIC and the OFC more robustly encoded the categorical distinction between water and sucrose rather than specific concentrations

At a single neuron level, the aIC and OFC Stimulus-encoding cells encode information in a categorical (water vs sucrose) and gradual (six concentrations) manner (**Figure 2**). The Categorical Stimulus-encoding subset was determined from auROC analyses, while a linear correlation was employed to identify the best Intensity Stimulus-encoding time window. Next, using a Support Vector Machine (SVM) decoder, we evaluated whether the already auROC-identified Stimulus-encoding cells also contain Stimulus information at the neuronal population level. We also assessed the impact of using linear vs. non-linear kernels on the SVM Stimulus-decoding performance. For each cortical area, we fed the activity of the auROC-identified Stimulus-encoding neurons, one vs. one, 8-fold cross-validated SVM classifier that decoded the identity of the Stimulus (the class) presented in each trial. The algorithm splits the multi-class classification into one binary classification problem per each pair of classes. The proportion of in-fold trials correctly classified by the model trained on the out-of-fold trials was considered a measure of decoding performance. We used linear, Gaussian, or third-order polynomial kernels to compare the SVM performance. The first kernel is mainly preferred for classification problems in which data is linearly separable; Gaussian and polynomial performs non-linear data transformations and are employed when a non-linear relationship between features exists (Ben-Hur et al. 2008). The linear kernel was not outperformed by the Gaussian or polynomial kernels, suggesting the data was linearly separable (**Figure 3 supplementary 1A**); thus, we will focus on the linear-kernel SVM results. The Stimulus-decoding accuracy was generally higher for the OFC compared to aIC and remained below 0.4 (the chance level for six stimuli is 0.166). Also, a difference in the encoding latencies was measured, with aIC leading the OFC. For comparison, we trained the SVM to classify the trials as pure water vs. sucrose stimulus employing the activity of the same selective neurons (**Figure 3 supplementary 1A**). Here, the decoding accuracy in both cortical regions reached around 0.75 (the chance level for two stimuli is 0.5, **Figure 3 supplementary 1B**). Altogether, aIC and OFC Stimulus-encoding cells represent categorical and intensity information at the single unit and the population levels, with the categorical feature being the prevailing contained information. Thus, when employing the activity of the same neurons, the SVM performed better in decoding the water-sucrose distinction than in decoding the six stimuli in both aIC and the OFC.

One caveat to this analysis is that it was done on the activity of relatively few cells that were already screened by their single-unit selectivity to the Water vs. Sucrose Stimulus conditions. Therefore, we additionally employed ANOVA on all recorded single-units to identify all the neurons with significant FR differences between the six stimulus concentrations and ran the same SVM decoding analysis. This approach allowed us to exploit all the possible information in the neural populations. We excluded the neurons with significant Choice-encoding, according to the Choice Probability index from the analysis, to minimize the potential contamination from neural signals associated with the subject's Choices (see Methods). A total of 154 aIC and 181 OFC neurons were identified. Using these expanded neural populations resulted in similar qualitative results (**Figures 3A and 3C**), suggesting that the neurons identified by the auROC analyses have as much information as the extended populations. More importantly, these observations corroborate our findings: the stimulus categorical distinction, water vs. sucrose, is more robustly represented compared to the gradual intensity representation of all stimulus concentrations.

To unveil the contribution of each stimulus over the linear-SVM decoder accuracy (**Figure 3A**, black line), we computed the proportion of trials in which each concentration was correctly classified. A decoder accuracy value of 0.5 indicates that the decoder correctly classified that concentration in half of the trials. It now can be seen that for aIC and the OFC, Water-Stimulus had the highest proportion of correctly classified trials. In OFC, though, the highest Sucrose concentration also exhibited a comparable proportion of correctly classified trials. Overall, in these gustatory cortices, both water and 20% sucrose were the stimuli most likely to be classified as correct**.** In sum, in a taste perceptual decision-making task, the Intensity information of the easiest-to-detect stimuli is represented more prominently at the aIC and OFC population levels. By using a larger subset of neurons, not only the auROC-identified Stimulus-encoding cells, we extend our results and confirm that identity (water vs sucrose) -and not the intensity- was the most important Stimulus information contained by the aIC and the OFC populations.

During the Response epoch, categorical decisions were sequentially represented by aIC and OFC neurons

Having encountered aIC and OFC subsets that, during the Stimulus epoch, contained information about Stimulus identity and intensity at the single-unit and population levels, we now went to seek whether the subject’s Response/Choice is represented during the Response epoch (-300 ms to +800 ms after last lick in Stimulus spout). To identify Choice-encoding cells, we performed the sliding-window auROC analysis and compared the FR of Water- vs. Sucrose-Response trials. The best time-window for categorical Choice-encoding was computed as described in the above section. Next, we identified the window whose activity significantly

correlated with the subject's Choice for each concentration see (Fonseca et al., 2018). In total, 117 of 388 (30.15%) aIC cells and 145 of 422 (34.36%) OFC cells significantly encoded the perceptual Choice/Response of the rats, regardless of the actual Stimulus delivered. **Figure 4A** depicts representative Choice-encoding neurons from the aIC and the OFC. The aIC Choice-encoding neuron exhibited a first peak of activity similar for all Stimuli right after the rat exited the central port and most likely already made a choice. This neuron also showed a second peak of activity around 400 to 600 ms, which was Choice-selective (see cyan asterisks; **Figure 4A**, left panel). This aIC neuron remained silent during Water-Response trials (see solid lines) but was active during Sucrose-Response trials (dashed lines), regardless of the Stimulus delivered at the central port, including Water-Stimulus (i.e., an incorrect trial; see blue dashed line). The OFC Choice-encoding cell displays a similar activity pattern (**Figure 4A**, right panel). **Figure 4B** depicts the neurometric curves (red) computed with the neural activity indicated by the cyan-shaded rectangles in **A**, and the corresponding psychometric curves (black) calculated with the rat's Responses/Choices within the corresponding experimental sessions. The close correspondence between the neurometric and the psychometric curves indicates that the activity of these two neurons is highly related to the rats' decisions. From the 117 aIC Choice-encoding neurons, 51 neurons (43.6%) showed higher activity for Water-Responses, 51 (43.6%) for Sucrose-Responses, and 15 (12.8%) showed a shift in their response patterns during the trial (**Figure 4 supplementary 1A,** left panels). For the 145 OFC Choice-encoding neurons, 67 (46.2%) exhibited preferred activity for Water-Choices, 49 (33.8%) preferred Sucrose-Choices, and 29 (20%) showed a shift in their response patterns during the Response epoch (**Figure 4 supplementary 1A**, right panels). These "shifting" neurons dynamically encoded categorical choices. First, they preferred one choice and later switched to the second option. This evidence suggests that the taste system also uses a kind of mixed selectivity.

In order to unveil how choice neurons sequentially monitor this decision variable across time, we normalized them and plotted them in a color-coded heatmap. **Figure 4C** illustrates the matrices of auROCs of the peak latency-sorted Choice-encoding aIC and OFC cells. We found the SqI, the PE, and the TS indexes to be 0.63, 0.96, and 0.376 for aIC and 0.53, 0.989, and 0.284 for the OFC, suggesting that Choice representation was slightly more sequential in aIC than the OFC. We observed these sequences to be highly reproducible in different trial splits. For aIC and OFC neurons, the MSE between splits was 0.0036 and 0.0021, respectively; both highly improbable to result by chance ($p < 0.001$). The auROC values temporal pattern of Choice-encoding cells shows that the choice information increases as the subject exits the Stimulus spout (**Figure 4D**); nonetheless, unlike Stimulus-encoding during the Stimulus epoch, we found no significant differences in the temporal activity patterns peak-encoding-times of Choice-encoding cells in the aIC compared to the OFC (**Figure 4E**; Two Sample Kolmogorov-Smirnov test, $p = 0.07$). Said that in **Figure 4E,** we notice an earlier slight bump in the number of Choice-encoding cells

in OFC compared to aIC (-200 to 100 ms) that was then over-passed by the aIC (400-800 ms) after the last central lick. These suggest that both taste cortices sequentially represented Choice and were recruited with a mark overlapped.

While reward Outcome was encoded less sequentially compared to Stimulus and Choice, taste cortex neurons in both regions exhibited rapid and parallel encoding of reward outcomes

Finally, utilizing a similar auROC analysis, we quantified the neurons that distinguish reward delivery or omission during the Outcome epoch, from -300 to +800 ms after the second lick on the Response spout, the feedback time. We found Outcome-encoding cells in both aIC (210 of 388, 54.12%) and OFC (231 of 422, 54.74%). These neurons exhibited a selective activity for correct vs. incorrect trials, irrespective of the Stimulus delivered. Overall, Outcome was the variable represented by the largest subset in both gustatory cortices, compared to the Stimulus- and Choice-encoding subsets size.

Next, we illustrate the activity of two representative Outcome-encoding neurons (**Figure 5A**) whose activity was aligned with the Outcome epoch start (feedback time). Both cells exhibited higher activity during correct compared to error trials (solid vs. dotted lines); noteworthy, within the same Outcome condition (correct vs. incorrect), the activity pattern during all six Stimulus trial types (0-20%) is highly similar. Interestingly, aIC cell activity (left panel) was also related to the rat's Responses prior to the feedback. Specifically, it exhibited higher activity for “Sucrose” Choices, regardless of whether they were correct or incorrect (see arrow **Figure 5A**, left panel); after the feedback, its activity became more influenced by the Outcome: higher activity for correct trials and lower for incorrect trials (see cyan-shaded rectangle). Similarly, the OFC Outcome-encoding cell responded more when the reward was delivered than when it was omitted (**Figure 5A**, left panel).

Interestingly, both neurons exhibited a diminished activity peak when the rats received water as a reward in the Water-Response spout compared to when they received it in the Sucrose-Response spout (blue vs. red solid lines, **Figure 5A**). Even though the reward is the same quality and volume in both Response spouts (3 drops of water), their neural responses are slightly different. These results suggest that some cortical neurons could also discriminate between water as a reward depending on the spatial location (lateral spouts) from which they obtained the reward. The cause remains unclear, but one possibility is a subtle difference in drinking position or that this activity, besides encoding reward delivery, also encodes spatial location. Notably, this phenomenon has been previously observed (MacDonald, et al., 2009).

Figure 5B shows the probability of correct responses as a function of Stimulus concentration calculated from the subjects' behavioral performance (black) and decoded from the neural activity indicated by the cyan rectangle in panel **A**. Both the neurometric curves and the high auROC values suggest that the activity of these neurons is highly related to the outcome. In aIC, 81 (38.57%) neurons exhibited preferred activity for incorrect trials (reward omission), 86 (40.95%) neurons showed higher activity for correct trials (reward delivery), and 43 (20.48%) neurons showed a shift in their response patterns (**Figure 4 supplementary 1**, lower panel left). In the OFC, 105 (45.45%) neurons showed higher activity in incorrect trials, 88 (38.1%) neurons had higher activity during correct trials, and 38 (16.45%) shifted their response patterns (**Figure 4 supplementary 1**, lower panel right). In each taste cortex, we recorded a similar proportion of neurons selective to reward omission or reward delivery, suggesting that rats could use both reward outcomes equally to solve the task.

Next, we explored sequential Outcome-encoding. The aIC and OFC Outcome-encoding were sorted by their peak auROCs and plotted in **Figure 5C**. These graphs show that the encoding of the Outcome is less sequentially structured than the Stimulus- and Choice-encoding (see **Figures 2C and 4C**) in both aIC and OFC. The SqI, the PE, and the TS indexes were 0.475, 0.983, and 0.23 for aIC and 0.467, 0.986, and 0.221 for OFC. The TS suffered the largest diminution, suggesting the outcome was encoded more extended than stimulus and choice. Conversely, we found the outcome encoding sequences to be highly reproducible between splits of different trials (aIC, MSE between splits: 0.003, $p < 0.001$; OFC, MSE between splits: 0.002, $p < 0.001$). **Figures 5D** and **5E** show the Outcome-encoding cells averaged auROC during the Outcome epoch and the cumulative distributions of the proportion of neurons that reached their peak auROC values across the Outcome epoch, respectively. We observed a rapid (after 50 ms) encoding of Outcome (reward delivery vs. omission) in both gustatory cortices. Moreover, we found no significant differences in the temporal recruitment of aIC and OFC Outcome-encoding cells (**Figure 4E**; Kolmogorov-Smirnov, $p = 0.23$), suggesting a parallel recruitment and brain-wide representation of Outcome (Laboratory et al., 2023) across gustatory cortices.

All relevant task variables are reflected in the Principal Components of the aIC and the OFC population activity

The previous analyses show that neural subpopulations in aIC and the OFC carry information related to the main events in the task. A remaining question is the weight of this information in the whole neural activity of aIC and the OFC. To get an insight, we performed PCA on the activity of all the neurons recorded (including the ones not previously included in the analysis) in each cortical area and searched for the Principal Components (PCs) that explained the most variability in the data and their

relationship to variables of the task. Importantly, we computed the PC employing the neural activity averaged over the different trials of the relevant task conditions (see below and Methods). Consequently, the neural trajectories reflect the mean trends and exclude the variability across trials.

The upper panels in **Figure 6A** show the main PCs computed from the activity of 360 aIC (left panel) and 441 OFC neurons (right panel) from 50 ms before to 800 ms after the stimulus delivery. These PCs explain 30.2% and 26.9% of the total variance in the neural activity of each taste cortex. In the figure, the different colors indicate the six stimulus conditions. In both cortical areas, the trajectories diverged after the stimulus delivery, reflecting the stimulus's identity. For aIC, the divergence began and accumulated soon after stimulus delivery. In contrast, the divergence started later and was less gradual for the OFC. Remarkably, these observations coincide with the time series of average auROCs and the cumulative latency distributions shown in **Figures 2D** and **2E**. In addition, it is worth noting that in the aIC, the population trajectories of the sucrose concentrations appear to cluster together, except for the pure water condition.

On the contrary, in the OFC, all the trajectories are more concentration-dependent in the population-state space, with water and 20% sucrose in opposite sites. To quantify this, we calculated, for each area separately, binned Euclidean distances between the trajectories of pairs of stimuli conditions. We distinguished two types of distances: the distance between the pure water condition and any sucrose condition (water-sucrose) and the distances between all the stimuli conditions (six stimuli). **Figure 6B** shows the mean ± SEM of these distances. In the aIC, both distances show an early increase between 100 and 150 ms after the stimulus delivery, but soon after, the water-sucrose distance became dominant over information-discriminating sucrose concentrations. In contrast, in the OFC, the PCA trajectory exhibited a delayed onset (250 ms) for discriminating stimuli information. Still, both distances (water vs. sucrose or all six stimuli) were similar across the period shown, corroborating that the OFC trajectories were more spread and dependent on concentration than in the aIC at the population neural-state space. Our results revealed that the aIC discriminated between taste stimuli earlier than the OFC. However, the OFC subsequently encoded more information about sucrose concentrations (perhaps reflecting its hedonic value) than the aIC.

The panels of **Figure 7** depict the projections of three PCs calculated from the activity of 236 aIC (upper panels) and 191 OFC neurons (lower panels), aligned to the time of the trial's feedback (the moment of reward delivery or omission). In this case, the activity was segregated into twelve conditions, resulting from combining the six stimuli and the two outcomes (correct or incorrect trials). Note that both the choice and the outcome are reflected in the divergence of the trajectories. For example, for aIC (upper panels in **Figure 7**), the PC 1, which explains 18.5% of the

total variance, shows trajectories that segregate completely into correct and incorrect trials soon after feedback (water reward delivery or omission). In contrast, for the same cortical area, the trajectories of the PC 2 are first segregated according to the rat's decision ('water' or 'sucrose' responses, see arrow), but soon after the time of feedback, they reconfigured, so the component now reflects the outcome, i.e., whether or not the trial was rewarded. Note that the reconfiguration is associated mainly with a 'switch' in the trajectory of the pure-water condition. This PC is very similar to the pattern of activity of the single neuron depicted in **Figure 5A**. The PC 5 from aIC is also related to the choice of the rats (see arrow). For the OFC (see lower panels in **Figure 7**), the PCs 1 (13.6%), 3 (7.8%), and 4 (6.11%) are shown. PC 1 and PC 3 trajectories were segregated according to correct and incorrect trials late or soon after the feedback. In contrast, trajectories in the PC 4 segregate according to the rat's choices (see arrow) in the time preceding the feedback. Note that the categorical choices are reflected in the OFC earlier than in aIC (compare PC 4 from OFC to PCs 2 and 5 from aIC).

From the PCA, we can conclude that the stimulus, the choice, and the outcome are the primary information encoded in the aIC and the OFC while performing the sucrose categorization task. Second, while the stimulus-related activity emerges earlier and more gradually in aIC than in the OFC, the choice-related activity emerges earlier in the OFC than in aIC, as the single-cell analyses suggested. Third, an essential component in aIC switches between choice and outcome representation by dynamically reconfiguring after the trial's feedback, consistent with the similar pattern observed in the activity of some single aIC neurons. Collectively, PCA population analysis recapitulated most, if not all, the encoding properties observed in single neurons.

Discussion

Our study investigated how the brain categorizes taste. We found that neurons in the anterior Insular Cortex (aIC) and the Orbitofrontal Cortex (OFC) prioritized distinguishing water from sucrose solutions rather than specific sweetness levels. Interestingly, the aIC encoded this categorization faster (within 200 ms) than the OFC (over 200 ms). Notably, in contrast to what has been observed in other species solving perceptual decision-making tasks, aIC and OFC neurons encoded both Stimulus and Choice. In monkeys detecting somatosensory stimuli, for example, there is a transition from stimulus to choice encoding across the brain hierarchy, where a parameterized representation of the stimulus is found in the neural activity of the primary sensory cortices and the neural activity in frontal areas is more related to encoding the subject’s decision (Romo and de Lafuente, 2013). In rats, we found that both regions maintained similar encoding of the rat's choices throughout the experiment. Moreover, we observed that choice information arose earlier in the OFC than in the aIC, which agrees with our previous study (Fonseca et al., 2018). Our results suggest that the aIC and the OFC interchange information about sensory

(first in the aIC) for decision variables (from the OFC) to perform distributed sensorimotor transformations as taste acquires behavioral meaning. A novel finding was that neurons in gustatory cortices encoded taste and choice information sequentially, as in a “relay race” of encoding cells. This dynamic and sequential encoding suggests that the brain does not rely on static, long-lasting representations of taste. Instead, information appears to be updated as the trial progresses. This is the first demonstration that the gustatory system used a "dynamic code” (Stroud et al., 2024), sometimes named mixed-selectivity (Lundqvist et al., 2018), and single-cell recordings, population decoding, and principal component analyses confirmed this conclusion. Furthermore, aIC and the OFC rapidly and in parallel encoded reward outcomes (correct vs. incorrect choices) within 150 ms. This reinforces the idea that gustatory cortices process taste information and play a role in categorizing choices and rapidly detecting reward outcomes**.**

We previously reported that the activity of aIC and OFC neurons of rats performing sucrose discrimination and generalization tasks encoded the stimulus intensity (the subjective perception of sucrose concentration), the subject's choices, the direction of the response movement, and the reward outcomes (delivery or omission) (Fonseca et al., 2018). Nevertheless, some questions remained unanswered. For example, it was unknown how sharp the neural representation of sucrose intensity is. In other words, are the different sucrose concentrations precisely discriminated by neural activity? Likewise, the behavioral importance of these theoretical parametric representations has not been quantified. In addition, the temporal encoding patterns of single neurons in the gustatory cortices and how these patterns are reflected in low-dimensional representations of population activity have not been described in the context of decision-making. To address these questions, we analyzed the activity of aIC and OFC neurons of rats performing a new sucrose categorization task with time-resolved decoding techniques and PCA.

Previous experiments in monkeys and rats passively receiving tastants found neurons in the taste cortex with concentration-dependent responses to sucrose, glucose, and other tastants or tastant mixtures; see, for example, (Rolls, 2023; Scott et al., 1991; Thorpe et al., 1983) for studies in monkeys and (Maier and Katz, 2013; Stapleton et al., 2006) for studies in the rat. Considering these antecedents, we expected a sharp encoding of the stimuli identity in our study. Nevertheless, we found that the distinction between water and sucrose (quality-related encoding), not the identity of the different stimulus (i.e., the sucrose concentrations), was the most relevant stimulus-related information in the population activity of aIC and OFC neurons. In our study, the average activity of some single neurons and the PC trajectories computed on the population activity tended to be modulated by the six stimuli (**Figures 2A, 2B, and 6A**). Despite this, our population trial-by-trial SVM decoding of the six sucrose concentrations was relatively poor compared to the decoding of water vs sucrose (**Figure 3 and Figure 3 Supplementary 1**). The weak encoding of the different sucrose concentrations probably resulted from overlapping firing rates across stimuli conditions and the neural response variability across trials

(**Figure 2B**). Notably, the encoding properties of the neural populations matched the behavior of the rats. Across animals and sessions, the psychophysical performance suggests that rats segregated three stimuli groups: a group including the three largest sucrose concentrations, all with similar probabilities of being categorized as 'sucrose'; a group with the 0% concentration alone with the lowest probability, and an intermediate group, including the 0.5 and 1.3% concentrations with probabilities closer to chance (**Figure 1B**). This behavior suggests a robust neural encoding of the extreme stimuli with a blurry limit in the middle of the stimulus range and matched well with the neural decoding and PC trajectories, especially with that of OFC (**Figure 3B right panel; Figure 6A right panel**).

There are many possible explanations for the discrepancies between the previous studies proposing the existence of a parametric representation of tastant concentrations and our study. First, most studies were based only on correlation or regression analyses on the activity of single neurons, and no attempts were made to decode the different stimuli. Also, these studies found a relatively small proportion of neurons with significant correlations/regressions between the tastant concentration and the neural firing rate (from 0.6% to 6.45% of the total recorded neurons; a study reports only three neurons and does not calculate the proportions of responsive neurons (Thorpe and Rolls 1983)). Thus, in contrast to ours, previous studies did not directly compare the relative strength of each encoding schema.

Here, a caution note is required; as we analyzed the activity of neural pseudo-populations, the encoding of the different stimuli could have been lost because of the variable duration of the different trials (Williams et al., 2020). A related alternative is that stimulus encoding might not reside in the firing rate alone. Previous studies proposed that spike timing, besides firing rate, may play a local role in taste processing (Di Lorenzo et al., 2009; Fonseca et al., 2018; Gutierrez et al., 2010). Our data did not rule out that spike timing could contain additional information to distinguish specific concentrations. To test these possibilities, simultaneous recordings, unsupervised time-warping methods, and spike-time-based analysis are required. Alternatively, aIC and OFC activity perhaps prioritized categorization stimuli information over specific taste concentration because of the behavioral context (Coss et al., 2022). To solve our categorization task, rats only need to distinguish water from sucrose, regardless of the concentration, and thus, the intensity attribute is not entirely relevant to solving this task. Perhaps in a discrimination sweet intensity task (Fonseca et al., 2018), in which the sweet intensity attribute becomes essential to solve it, gustatory cortices pay more attention to this sensory attribute. If true, it would further suggest that the activity of gustatory cortices could be context-dependent, and thus, it changes depending on the demands of the behavioral task (Talpir and Livneh, 2024).

Our study further confirmed that taste coding is sparse and distributed, with only a few neurons carrying information about taste stimuli (Chen et al., 2020; Fonseca et al., 2018). As shown in **Figure 2B** and our previous work (Fonseca et al., 2018), we identified a small population of cortical sensory neurons (<18%) that linearly tracked sucrose concentrations both during increases (reflecting changes in intensity) and decreases (possibly reflecting changes related to osmotic pressure (Hanamori, 2001; Lyall et al., 1999) or the washing out of bicarbonate ions in saliva (Zocchi et al., 2017))—rationalizing why we observed robust responses to distilled water in our categorization task that might overshadow the sparse monotonic responses to sucrose concentration. These water responses (either as stimuli or as rewards) further support the idea of water as an independent taste quality (Rosen et al., 2010).

Our data also showed that water-evoked responses, mainly when used as a reward (in lateral spouts), are more complex and could not be merely explained by oral, osmotic, or pure taste factors. This is because neural activity in both taste cortices was slightly different if rats drank water from the left or right spout (MacDonald et al., 2009), suggesting that reward expectation (Mazzucato et al., 2019), differences in body position, or perhaps more likely ipsi- or contralateral tongue movements (either left or right spouts (Li et al., 2015)) modulate taste evoked responses.

In an active decision-making behavioral context, we also observed that the rat's brain seems to follow a general brain-wave like activation pattern reflecting sensorimotor transformations from stimuli to decision-making (Arroyo et al., 2024; Laboratory et al., 2023). Specifically, the brain wave is triggered by sampling the stimuli that initially recruit a small number of neurons, but then more and more neurons take part in encoding choice, anticipation, and reward outcome, in which this wave dissipates. Impressively, this wavelike recruitment seems to be brain-wide and distributed phenomenon, as it has been reported that it occurs in parallel in multiple cortical and subcortical brain regions (Arroyo et al., 2024; Fonseca et al., 2018; Gutierrez et al., 2010; Laboratory et al., 2023; Musall et al., 2019; Steinmetz et al., 2019), substantiating its importance for active sensory processing and decision making. More importantly, our results demonstrate that aIC and the OFC are not passive primary or secondary sensory cortices, in agreement with previous observations (Fonseca et al., 2018; Gutierrez et al., 2010; Juen et al., 2024; Vincis et al., 2020). Our findings go beyond showing the aIC and OFC's involvement in taste processing. These regions actively participate and interact in the entire behavioral response, from initial taste perception to taste-guided decisions, using dynamic coding and moving bumps of encoding sequences.

A novel finding was that both aIC and the OFC sequentially and dynamically represented taste and choice information, with different neurons encoding information at different times, and these 'encoding sequences' were reproducible across subsets of trials. This phenomenon may appear similar to the cell assembly sequences described in many previous studies. In the cell assembly sequences, the neurons activate in sequence, creating reproducible patterns across trials of the

same experimental conditions. The sequences are characterized by a unique combination of active neurons at each time point, and from the current pattern of active neurons, one can decode temporal information or information that systematically develops over time (Eichenbaum, 2014; Pastalkova et al., 2008; Zhou et al., 2020). Our study showed sequences of information encoding, not neural activation. In the former case, the activity of each neuron was selective to specific task variables, and different neurons maximally encoded such information in different periods, generating a sequence of information maintenance. In these encoding sequences, the activation periods are not necessarily encoding periods (See, for example, the neural activity depicted in **Figure 4A**). Similar sequences have been shown, for example, for the encoding of choice in the parietal cortex of rats in navigation decision tasks (Harvey et al., 2012). In their case, sequences were proposed to keep the information for working memory and movement planning during navigation. Our study shows that these sequences are not restricted to navigation contexts. Another hallmark of dynamic encoding is that individual neurons change their tuning patterns (Lundqvist et al., 2018). We found that some neurons inverted their mixed-selectivity pattern. Some category-selective neurons, for example, initially showed higher activity for the 'water' response trials, but later, during the trial, their response was higher for the 'sucrose' response trials (**Figure 2 Supplementary 1**. Upper panels). Some outcome-selective neurons also showed this encoding switching (**Figure 4 Supplementary 1**). A more complex switching pattern was that of some aIC neurons that changed from choice to outcome encoding (**Figure 5A**). Interestingly, this change was systematic. Before feedback, the activity during the 'water' correct responses was more similar to that of the 'water' incorrect responses, and that of the 'sucrose' correct responses was more similar to that of the 'sucrose' incorrect responses, thus reflecting the response of the animals. After feedback, only the 'water' incorrect and correct responses changed, so now the overall activity reflected the trial's outcome (**Figure 5A**). This effect was robust enough to be seen at the population level in the PCA (see PC 2 in **Figure 7** upper panel). The relevance and neural underpinnings of dynamic coding are still debated (Stroud et al., 2024). Dynamic coding emerges in complex tasks with multiple stimuli (Lundqvist et al., 2018). A recent modeling study found that the emergence of dynamic codes depends on the temporal complexity of the task, the variability of delay durations, the strength of neuron coupling, prior training in another task, and the presence or absence of task-irrelevant, motion-related dynamic cues (Orhan and Ma, 2019). Studies comparing tasks with diverse complexity and structure will shed more light on these questions.

In conclusion, in a new paradigm of categorizing different sucrose concentrations, the firing rate of aIC and OFC neurons did not maintain a sharp, parametric representation of the different concentrations but a robust, gross distinction between sucrose and non-sucrose solutions. In addition, the information relevant to the task was not maintained by long-lasting firing rate codes but by sequences of information encoding in which the firing rate of different neurons represented the relevant

information at different and relatively short periods during the trial. aIC and OFC neural populations also showed changing patterns of mixed-information encoding, another hallmark of dynamic encoding. These observations increase our knowledge about the use of taste information and how it is transformed into taste guided decisions.

Materials and methods

Subjects. Male Sprague-Dawley rats (n = 11) weighing 300–320 g at the beginning of the experiment were trained. The subjects were individually housed in cages in a temperature-controlled (22 ± 1°C) room, with a 12:12 h light-dark cycle (lights on at 0700) and *ad libitum* access to food (PicoLab Rodent Diet 20, St. Louis, MO, USA). Experiments were conducted at the same time within the light-dark cycle (1400 to 1900 h). After each experiment, the rats were given free access to water for 30 min. The CINVESTAV Institutional Animal Care and Use Committee approved all the experimental procedures.

Apparatus. Standard operant conditioning chambers were employed (30.5 x 24.1 x 21.0 cm, Med Associates Inc, VT, USA). The front panel of each chamber was equipped with one central and two laterals V-shaped lick spouts with a photobeam sensor to register individual licks (Med Associates Inc, VT, USA). The central spout comprised a bundle of 6 blunted needles (20-gauge) glued at the tip of a stainless-steel sipper tube, while each lateral spout comprised one needle. Each needle was independently connected to pressurized liquid reservoirs using a silicone tube, resulting in an eight-channel fluid delivery system (Fonseca et al., 2018). By turning on and off independent solenoid valves (Parker, Ohio, USA), the system allowed the delivery of controlled volumes of liquid in each spout. One of the six needles in the central spout delivered the Stimulus concentrations, while water Reward was delivered in the lateral spouts. On the rear panel, there was an ambiance white noise amplifier with a speaker that was turned on during all sessions. Chambers were enclosed in a ventilated sound-attenuating cubicle. Experimental events were controlled and registered by a computer via a Med Associates interface (Med Associates Inc, VT, USA).

Stimuli. Six solutions (0, 0.5, 1.3, 3.2, 7.9, and 20 w/v%) of sucrose (reagent-grade, Sigma-Aldrich, Mexico) were diluted in distilled water. All sucrose concentrations were prepared every other day, maintained under refrigeration, and used at room temperature during the experiments.

Sucrose categorization task. Rats were trained in a two-alternative forced-choice task to report the presence or absence of sucrose in a 10-μL Stimulus drop. The trial structure is as follows: rats were required to reach and dry-lick the Stimulus spout a variable number of times (between two or three) to receive a 10-μL liquid drop (Stimulus delivery) (**Figure 1A**). The Stimulus could be one of six sucrose

concentrations: 0, 0.5, 1.3, 3.2, 7.9, and 20%. Subsequently, the subject had to move and dry-lick the lateral Response-Spout associated with the Stimulus received: Water-Stimulus → Left Response-Spout; Sucrose-Stimulus → Right Response-Spout. These conditions were counterbalanced; thus, we will refer to Response spouts as Water- and Sucrose-Response spouts. If the rat licked the correct Response spout, the subsequent three licks resulted in the delivery of one drop of water per lick as a reward; otherwise, for error trials, the lights went off and on, and no reward was provided. The moment of reward delivery or omission is designated as the time of feedback. In each experimental session, water (0% sucrose) was delivered as the Stimulus in 50% of the trials, and the remaining concentrations were homogeneously distributed over the remaining trials. The learning criterion was 80% correct responses during four consecutive sessions.

Electrode implantation. Once animals achieved the learning criterion, custom-made, 4 x 4 tungsten wire electrode arrays were implanted in the anterior Insula Cortex (aIC, n = 6) or the Orbitofrontal Cortex (OFC, n = 5) under ketamine/xylazine anesthesia (70 mg/kg/20 mg/kg, i.p.,(Gutierrez et al., 2010)). Implantation coordinates were: aIC, +1.6 to +2.3 mm AP, +5.2 mm ML from bregma, and -4.6 to -4.7 mm DV from the dura; OFC, +3.5 mm AP, +3.2 mm ML from bregma, and -4.4 mm DV from the dura. After surgery, rats were given intraperitoneal enrofloxacin (0.4 ml/kg) and ketoprofen (45 mg/kg) for three days and one week of rest for recovery.

Electrophysiology. Extracellular voltage signals acquired by a MAP system (Plexon, Dallas, TX) were amplified x1 (analog headstage, Plexon HST/16o25-GEN2- 18P-2GP-G1), x1000 and sampled at 40 kHz. Raw signals were band-pass filtered (154 Hz-8.8 kHz) and digitalized (12-bit resolution). The action potentials were isolated using voltage-time threshold windows and PCA in real-time. Waveforms were assigned to the same unit if not violated the refractory period (1 ms), and weather confirmed a neat delimited ellipsoid cloud on the first three Principal Components. Additional offline sorting was performed (Offline Sorter, Plexon, Dallas, TX), and only single units with a signal-to-noise ratio of 3:1 were analyzed (Fonseca et al., 2018; Gutierrez et al., 2010).

Histology. After the experiments were completed, subjects were administered an overdose of pentobarbital sodium (150 kg/mg, i.p.) and perfused transcardially with PBS (1x) followed by 4% PFA. Brains were removed, stored for 24 hrs in 4% PFA, and changed to a 30 v/v% sucrose/PBS solution. Coronal, 40-micron sections stained with Cresyl violet corroborated the recording locations (Fonseca et al., 2018).

Data analysis

Subroutines written in Matlab (Matworks v. 7.6.0.324) and the SPSS statistical package (version 20, SPSS Inc., Chicago, IL, 2011) were used for the statistical analyses. The level of statistical significance to reject the null hypothesis was $\alpha = 0.05$ unless stated otherwise.

Behavior

The psychometric curves for each session were built as the probability of selecting the Sucrose-Response spout ('p of sucrose response') for each Stimulus concentration. Power functions were fitted to these data, and the stimulus value at .5 probability of responding 'sucrose' was computed. The mean values of the psychometric curves oscillate between 0 and 1, but no Stimulus concentration leads to perfect categorization, not even the "obvious"/"easiest" concentrations of 0 and 20% sucrose. In order to corroborate that Stimulus presentations were balanced within sessions, we quantified the proportion of trials in which the subject received Water- or Sucrose-Stimulus. We also characterized the subject's Responses and their associated outcome distribution: we quantified the proportion of trials in which the subject reported perceiving the stimulus as Water or Sucrose (Water- vs. Sucrose-Response) and the proportion of these trials that were rewarded. Finally, we evaluated the effect of stimulus concentration over the time of licking in the stimulus and response spouts and the time to move from the stimulus to the response spout. Specifically, for each Stimulus concentration, we computed the time elapsed between Stimulus delivery to the last lick emitted in the Stimulus spout (center licking), the time elapsed between the first and last lick in the Response spout (lateral licking), the time between the last Stimulus spout lick and first lateral lick spout (movement time).

Encoding of the task's variables

For each neuron and trial, firing rates were computed in 100-ms size windows moving in 10-ms steps. These data were employed for the analyses described below.

Single neuron encoding of the Stimulus quality (Water vs Sucrose)

To determine the relation between neural activity and the task's parameters, we employed auROC analyses. For Stimulus encoding, we constructed two firing rate distributions, one with the activity of each neuron during Water- or Sucrose-Stimulus trials; all sucrose concentrations are embedded in the Sucrose category. The auROC measures the overlap between the two distributions, with ranging values from 0 to 1, where the edge values 0 and 1 signal complete segregation of the distributions, and 0.5 indicates complete overlap. It is important to note that, in tasks like ours, a trial-by-trial correlation between Stimulus and Responses emerges when analyzing only correct trials. Consequently, differentiating the neural activity associated with the Stimulus from the activity related to the subject's Response is a common problem. We addressed this problem by computing two auROC values from the same trials for each neuron and time bin. The firing rate distributions were arranged according to the presented Stimulus or the Responses reported by the subjects. Then, we compared both auROC values and considered putative Stimulus-

encoding the bins with the Stimulus-auROC higher than 0.6 (or lower than 0.4) and higher (lower) than the corresponding Response-auROC. The auROC values of 0.4 and 0.6 roughly corresponded to the values at 0.25 and 0.95 in the distribution of auROC values from all the time bins and cells included in this analysis. Ten thousand permutations of the Stimulus labels were employed to build null distributions per time bin to identify the bins with Stimulus-auROCs above chance ($p \leq 0.05$). Neurons with at least five consecutive significant bins were considered to encode Stimulus information.

Single neuron encoding of the subject's Response

To identify cells encoding the perceptual choice of the subjects, we performed auROC analysis on the distributions of firing rates associated with 'Water' or 'Sucrose' Response trials. This index reflexes the proportion of behavioral responses that can be predicted from single neuron activity. By including correct and error trials in the analysis, the index eliminates the trial-by-trial correlation between the presented stimulus and the subject's choices when analyzing only correct trials (Britten et al., 1996; Romo et al., 2004). For each neuron and time bin, we constructed two firing rate distributions, one containing the firing rates of the trials where the rats chose the 'water' response and another with the firing rates of the trials where the rats chose the 'sucrose' response. Trials of any stimulus condition could contribute to one or another distribution. From these distributions, the area under the ROC curves was calculated. A resulting value of 0.5 indicates a complete overlap between the distributions, whereas values of 0 or 1 indicate a complete separation. Neurons with five consecutive bins with a choice probability larger than 0.6 or lower than 0.4 and surpassing a two-tailed permutation test (10,000 permutations) were considered to encode the choice of the animals significantly. The auROC values of 0.4 and 0.6 roughly corresponded to the values at 0.25 and 0.95 in the distribution of auROC values from all the time bins and cells included in this analysis.

Single neuron encoding of the trial's Outcome

To identify cells encoding the Outcome, we calculated the Outcome-auROC values by comparing the firing rate distributions of rewarded vs. non-rewarded trials. Outcome-encoding neurons are determined using the same significant criterion described above.

Sequences of encoding by single neurons

The temporal profile of Stimulus, Choice, and Outcome encoding in the cell populations seemed to differ, being more sequential for Stimulus and Choice than for Outcome in both aIC and OFC (see **Figures 2C and 3C**). To quantify this effect, we applied indices of peak entropy and temporal sparsity (Zhou et al., 2020) to the auROC values associated with significant Stimulus, Choice, and Outcome encoding across time bins for cells in aIC and OFC (**Figures 2C and 3C**). Here, peak entropy determines how homogeneously the encoding periods of each neuron cover specific time ranges, with values close to one for more homogenous covering. Conversely, temporal sparsity measures the sharpness of the encoding periods, with short encoding periods associated with values close to one. Both indexes provide a measure of the sequentially (Zhou et al., 2020), in our case, of parameter encoding in the neural populations.

To evaluate the reproducibility of the sequences of neural encoding across different trials, we performed holdout cross-validation. First, we randomly partitioned the data from each neuron into two trial subsets and ran the ROC analysis separately for each data split and neuron. We constructed two matrices of population auROC values across time (matrices of cell by bin size). We then ordered the cells in matrix two by the indexes resulting from sorting the cells in matrix one by their latencies to peak auROC. Next, we calculated the mean-squared error (MSE; MATLAB immse function) between the two sorted matrices to measure pattern similarity. MSE close to zero implies that the population encoding dynamic is similar across the two data splits. A permutation test (10,000 permutations of the row indexes of matrix 2) allowed us to test the possibility that such similarity resulted from chance.

Support Vector Machine decoding of the Stimulus quality (Water vs. Sucrose) and intensity (all concentrations)

We used 8-fold cross-validated (*crossval* function, Matlab), one vs. one Support Vector Machine (SVM, *fitcecoc* function, Matlab) for decoding the Stimulus delivered in each trial. We trained the SVM to decode Water *versus* Sucrose, or the six Stimulus concentrations in 100-ms time windows, moving in 10-ms steps from -400 to 800 ms from the Stimulus delivery. We ran the SVM with linear, Gaussian, and third-order polynomial kernels. We took the classification loss from observations not used for training (1 – loss, *kfoldLoss* function, Matlab) as a measure of decoding accuracy. To compare the decoding accuracy across cortical areas and decoding schemas (Water *vs.* Sucrose or the six concentrations). For this purpose, the SVM was trained in the two decoded schemas with the same number of neurons, trials per neuron, and trials per decoded condition. For Water- and Sucrose-Stimulus decoding, 16 correct trials -8 trials per condition- were employed per SVM run. For decoding the stimuli, 48 correct trials per stimuli condition were used. Homogenizing the trial number required the selection of neurons with 2 x 8 correct trials when

arranged according to the binary decoding schema and 6 x 8 correct trials when arranged according to the other schema. Using the same neurons across the two decoding schemas allowed direct comparisons within cortical areas. Also, note that the employed trial's counts would have favored decoding the six concentrations. The number of neurons and trials was homogenized by random sampling with replacement across brain areas and neurons. Fifteen samplings for neurons and ten for trials were employed for 150 samplings. The decoding accuracy is reported as the mean (±SEM) of the 150 samplings. The Stimulus labels were permuted to calculate the chance of SVM performance. The permutation results are the mean (± SEM) Stimulus-decoding accuracy of 150 neuron/trial samplings. The whole analysis was first performed on the activity of aIC and OFC stimulus-encoding neurons from the Signal Detection Theory-based analysis. Next, the analysis was run on the activity of these cells and all the neurons with significant differences in a one-way ANOVA with the stimulus as the six-level factor. Neurons with significant Choice encoding, according to auROC, were excluded from the analysis.

Determining the effect of licking movements

To test whether the activity of the population of outcome-encoding neurons was more related to reward delivery/omission than to the licking behavior of the rats, we compared the performance of the population neural activity or the licking behavior in the trial-by-trial decoding of the delivery or omission of reward by an SVM. If the activity of the population of outcome-encoding neurons is independent of the licking behavior of the rats, then differences between the classification accuracy of both parameters are expected (Fonseca et al., 2018). First, we computed the firing rate (FR) of the outcome encoding cells in 100 ms time windows, moving in 10 ms steps from -400 to 800 ms from the trial's feedback. The lick rate (LR) was computed in sliding windows of the same size and steps as for the neural activity. Only neural firing and licking rates from the same sessions and trials were employed. As the times of licking varied from trial to trial, when all the session trials are used for the decoding, the licking movements tend to 'tile' all the post-feedback period. This could cause artificially continuous and high decoding performances when the SVM uses the licking rate. To avoid this problem, all the inter-lick intervals were normalized to 140 ms, and the spike times were warped to the normalized times. This procedure resulted in the alignment of the licking movements and the warping of the spike times in all the trials employed in the analysis. Next, we used a linear-kernel SVM (one vs. one, 8-fold cross-validated) for decoding the Outcome in each trial, utilizing the firing rate of the neural populations or the licking rate of the rats. We took the classification loss from observations not used for training to measure decoding accuracy for both FR and LR. The number of neurons and trials was homogenized by random sampling with replacement across brain areas and neurons (16 trials per neuron,

eight from correct and eight from incorrect trials) to compare the decoding accuracy across cortical regions. Fifteen samplings for neurons and ten for trials were employed for 150 samplings. Also, the stimulus labels were permuted to get an idea of the chance of SVM performance. Significant differences between the means of the two decoding accuracy distributions were determined across time by a bootstrap test (sample with replacement, 10,000 iterations).

PCA analysis and population trajectories

For each cortical area, Principal Component Analyses were run over the activity of all the recorded neurons averaged within the experimental conditions of interest: the presented stimulus (6 conditions), the animal's choice x presented stimulus (12 conditions), or the trial's outcome x presented stimulus (12 conditions). For these analyses, the times of action potentials of each neuron in each trial were aligned to the relevant behavioral event: the time of stimulus delivery, the time of the last lick in the central port, or the time of feedback. The activity was then convolved at 1ms resolution, with a 20 ms width Gaussian kernel employing the ksdensity function of MATLAB. The data was then converted to FR and averaged per neuron within the relevant experimental conditions. Only neurons with at least five correct trials per condition were included in the analysis focused on stimulus encoding. In the other analyses, we required at least two trials per condition per neuron.

The mean FR of all recorded neurons was arranged in a matrix of $n \times c$ with n = number of analyzed neurons and c = time bin x experimental condition. Covariance matrices were computed from these data and subsequently employed to compute PC coefficients.

Given a linear transformation of a matrix X into a matrix Y, such that each dimension of Y explains the variance of the original data X in descending order, PCA can be described as the search for matrix P that transforms X into Y as follows:

$$Y = PX$$

The principal component coefficients matrix P were multiplied by the X' matrix to transform the neural data into the space of the original Y. A locally weighted smoothing function was applied to the columns of the Y matrix. Selected dimensions of Y were plotted to generate graphical one-dimensional trajectories of the population neural activity (Mendoza et al., 2016).

References

Arroyo B, Lemus EH, Gutierrez R. 2024. The flow of reward information through neuronal ensembles in the accumbens. doi:10.1101/2024.02.15.580379

Barretto RPJ, Gillis-Smith S, Chandrashekar J, Yarmolinsky DA, Schnitzer MJ, Ryba NJP, Zuker CS. 2015. The neural representation of taste quality at the periphery. *Nature* **517**:373–376. doi:10.1038/nature13873

Britten KH, Newsome WT, Shadlen MN, Celebrini S, Movshon JA. 1996. A relationship between behavioral choice and the visual responses of neurons in macaque MT. *Visual Neuroscience* **13**:87–100. doi:10.1017/S095252380000715X

Chen K, Kogan J, Fontanini A. 2020. Spatially Distributed Representation of Taste Quality in the Gustatory Insular Cortex of Behaving Mice. *Current Biology*. doi:10.1016/j.cub.2020.10.014

Coss A, Suaste E, Gutierrez R. 2022. Lateral NAc Shell D1 and D2 Neuronal Ensembles Concurrently Predict Licking Behavior and Categorize Sucrose Concentrations in a Context-dependent Manner. *Neuroscience* **493**:81–98. doi:10.1016/j.neuroscience.2022.04.022

de Araujo IET, Kringelbach ML, Rolls ET, McGlone F. 2003. Human Cortical Responses to Water in the Mouth, and the Effects of Thirst. *Journal of Neurophysiology* **90**:1865–1876. doi:10.1152/jn.00297.2003

Di Lorenzo P, Chen J-Y, Victor J. 2009. Quality Time: Representation of a Multidimensional Sensory Domain through Temporal Coding. *The Journal of neuroscience : the official journal of the Society for Neuroscience* **29**:9227–38. doi:10.1523/JNEUROSCI.5995-08.2009

Eichenbaum H. 2014. Time cells in the hippocampus: a new dimension for mapping memories. *Nat Rev Neurosci* **15**:732–744. doi:10.1038/nrn3827

Fonseca E, de Lafuente V, Simon SA, Gutierrez R. 2018. Sucrose intensity coding and decision-making in rat gustatory cortices. *eLife* **7**:e41152. doi:10.7554/eLife.41152

Gutierrez R, Fonseca E, Simon SA. 2020. The neuroscience of sugars in taste, gut-reward, feeding circuits, and obesity. *Cell Mol Life Sci* **77**:3469–3502. doi:10.1007/s00018-020-03458-2

Gutierrez R, Simon SA, Nicolelis MAL. 2010. Licking-Induced Synchrony in the Taste–Reward Circuit Improves Cue Discrimination during Learning. *J Neurosci* **30**:287–303. doi:10.1523/JNEUROSCI.0855-09.2010

Hanamori T. 2001. Effects of Various Ion Transport Inhibitors on the Water Response in the Superior Laryngeal Nerve in Rats. *Chemical Senses* **26**:897–903. doi:10.1093/chemse/26.7.897

Harvey CD, Coen P, Tank DW. 2012. Choice-specific sequences in parietal cortex during a virtual-navigation decision task. *Nature* **484**:62–68. doi:10.1038/nature10918

Juen Z, Villavicencio M, Zuker CS. 2024. A neural substrate for short-term taste memories. *Neuron* **112**:277-287.e4. doi:10.1016/j.neuron.2023.10.009

Kogan JF, Fontanini A. 2024. Learning enhances representations of taste-guided decisions in the mouse gustatory insular cortex. *Current Biology*. doi:10.1016/j.cub.2024.03.034

Laboratory IB, Benson B, Benson J, Birman D, Bonacchi N, Carandini M, Catarino JA, Chapuis GA, Churchland AK, Dan Y, Dayan P, DeWitt EE, Engel TA, Fabbri M, Faulkner M, Fiete IR, Findling C, Freitas-Silva L, Gerçek B, Harris KD, Häusser M, Hofer SB, Hu F, Hubert F, Huntenburg JM, Khanal A, Krasniak C, Langdon C, Lau PYP, Mainen ZF, Meijer GT, Miska NJ, Mrsic-Flogel TD, Noel J-P, Nylund K, Pan-Vazquez A, Pouget A, Rossant C, Roth N, Schaeffer R, Schartner M, Shi Y, Socha KZ, Steinmetz NA, Svoboda K, Urai AE, Wells MJ,

West SJ, Whiteway MR, Winter O, Witten IB. 2023. A Brain-Wide Map of Neural Activity during Complex Behaviour. doi:10.1101/2023.07.04.547681

Lang L, Camera GL, Fontanini A. 2023. Temporal progression along discrete coding states during decision-making in the mouse gustatory cortex. *PLOS Computational Biology* **19**:e1010865. doi:10.1371/journal.pcbi.1010865

Lara AH, Kennerley SW, Wallis JD. 2009. Encoding of gustatory working memory by orbitofrontal neurons. *J Neurosci* **29**:765–774. doi:10.1523/JNEUROSCI.4637-08.2009

Li N, Chen T-W, Guo ZV, Gerfen CR, Svoboda K. 2015. A motor cortex circuit for motor planning and movement. *Nature* **519**:51–56. doi:10.1038/nature14178

Lundqvist M, Herman P, Miller EK. 2018. Working Memory: Delay Activity, Yes! Persistent Activity? Maybe Not. *J Neurosci* **38**:7013–7019. doi:10.1523/JNEUROSCI.2485-17.2018

Lyall V, Heck GL, DeSimone JA, Feldman GM. 1999. Effects of osmolarity on taste receptor cell size and function. *American Journal of Physiology-Cell Physiology* **277**:C800–C813. doi:10.1152/ajpcell.1999.277.4.C800

MacDonald CJ, Meck WH, Simon SA, Nicolelis MAL. 2009. Taste-guided decisions differentially engage neuronal ensembles across gustatory cortices. *J Neurosci* **29**:11271–11282. doi:10.1523/JNEUROSCI.1033-09.2009

Maier JX, Katz DB. 2013. Neural dynamics in response to binary taste mixtures. *Journal of Neurophysiology* **109**:2108–2117. doi:10.1152/jn.00917.2012

Mazzucato L, La Camera G, Fontanini A. 2019. Expectation-induced modulation of metastable activity underlies faster coding of sensory stimuli. *Nat Neurosci* **22**:787–796. doi:10.1038/s41593-019-0364-9

Mendoza G, Peyrache A, Gámez J, Prado L, Buzsáki G, Merchant H. 2016. Recording extracellular neural activity in the behaving monkey using a semichronic and high-density electrode system. *J Neurophysiol* **116**:563–574. doi:10.1152/jn.00116.2016

Musall S, Kaufman MT, Juavinett AL, Gluf S, Churchland AK. 2019. Single-trial neural dynamics are dominated by richly varied movements. *Nat Neurosci* **22**:1677–1686. doi:10.1038/s41593-019-0502-4

Nelson G, Hoon MA, Chandrashekar J, Zhang Y, Ryba NJ, Zuker CS. 2001. Mammalian sweet taste receptors. *Cell* **106**:381–390. doi:10.1016/s0092-8674(01)00451-2

Orhan AE, Ma WJ. 2019. A diverse range of factors affect the nature of neural representations underlying short-term memory. *Nat Neurosci* **22**:275–283. doi:10.1038/s41593-018-0314-y

Pastalkova E, Itskov V, Amarasingham A, Buzsáki G. 2008. Internally generated cell assembly sequences in the rat hippocampus. *Science* **321**:1322–1327. doi:10.1126/science.1159775

Perez IO, Villavicencio M, Simon SA, Gutierrez R. 2013. Speed and accuracy of taste identification and palatability: impact of learning, reward expectancy, and consummatory licking. *American Journal of Physiology-Regulatory, Integrative and Comparative Physiology* **305**:R252–R270. doi:10.1152/ajpregu.00492.2012

Rolls ET. 2023. The orbitofrontal cortex, food reward, body weight and obesity. *Social Cognitive and Affective Neuroscience* **18**:nsab044. doi:10.1093/scan/nsab044

Rolls ET, Yaxley S, Sienkiewicz ZJ. 1990. Gustatory responses of single neurons in the caudolateral orbitofrontal cortex of the macaque monkey. *Journal of Neurophysiology* **64**:1055–1066. doi:10.1152/jn.1990.64.4.1055

Romo R, de Lafuente V. 2013. Conversion of sensory signals into perceptual decisions. *Prog Neurobiol* **103**:41–75. doi:10.1016/j.pneurobio.2012.03.007

Romo R, Hernández A, Zainos A. 2004. Neuronal Correlates of a Perceptual Decision in Ventral Premotor Cortex. *Neuron* **41**:165–173. doi:10.1016/S0896-6273(03)00817-1

Rosen AM, Roussin AT, Di Lorenzo PM. 2010. Water as an Independent Taste Modality. *Front Neurosci* **4**. doi:10.3389/fnins.2010.00175

Samuelsen CL, Fontanini A. 2017. Processing of Intraoral Olfactory and Gustatory Signals in the Gustatory Cortex of Awake Rats. *J Neurosci* **37**:244–257. doi:10.1523/JNEUROSCI.1926-16.2016

Scott TR, Plata-Salaman CR, Smith VL, Giza BK. 1991. Gustatory neural coding in the monkey cortex: stimulus intensity. *Journal of Neurophysiology* **65**:76–86. doi:10.1152/jn.1991.65.1.76

Stapleton JR, Lavine ML, Wolpert RL, Nicolelis MAL, Simon SA. 2006. Rapid Taste Responses in the Gustatory Cortex during Licking. *J Neurosci* **26**:4126–4138. doi:10.1523/JNEUROSCI.0092-06.2006

Steinmetz NA, Zatka-Haas P, Carandini M, Harris KD. 2019. Distributed coding of choice, action and engagement across the mouse brain. *Nature* **576**:266–273. doi:10.1038/s41586-019-1787-x

Stroud JP, Duncan J, Lengyel M. 2024. The computational foundations of dynamic coding in working memory. *Trends in Cognitive Sciences* S1364661324000536. doi:10.1016/j.tics.2024.02.011

Talpir I, Livneh Y. 2024. Stereotyped goal-directed manifold dynamics in the insular cortex. *Cell Reports* **43**. doi:10.1016/j.celrep.2024.114027

Thorpe SJ, Rolls ET, Maddison S. 1983. The orbitofrontal cortex: neuronal activity in the behaving monkey. *Exp Brain Res* **49**:93–115. doi:10.1007/BF00235545

Vincis R, Chen K, Czarnecki L, Chen J, Fontanini A. 2020. Dynamic Representation of Taste-Related Decisions in the Gustatory Insular Cortex of Mice. *Curr Biol* **30**:1834-1844.e5. doi:10.1016/j.cub.2020.03.012

Vincis R, Fontanini A. 2019. Central taste anatomy and physiology. *Handb Clin Neurol* **164**:187–204. doi:10.1016/B978-0-444-63855-7.00012-5

Williams AH, Poole B, Maheswaranathan N, Dhawale AK, Fisher T, Wilson CD, Brann DH, Trautmann EM, Ryu S, Shusterman R, Rinberg D, Ölveczky BP, Shenoy KV, Ganguli S. 2020. Discovering Precise Temporal Patterns in Large-Scale Neural Recordings through Robust and Interpretable Time Warping. *Neuron* **105**:246-259.e8. doi:10.1016/j.neuron.2019.10.020

Wu A, Dvoryanchikov G, Pereira E, Chaudhari N, Roper SD. 2015. Breadth of tuning in taste afferent neurons varies with stimulus strength. *Nat Commun* **6**:8171. doi:10.1038/ncomms9171

Zhou S, Masmanidis SC, Buonomano DV. 2020. Neural Sequences as an Optimal Dynamical Regime for the Readout of Time. *Neuron* **108**:651-658.e5. doi:10.1016/j.neuron.2020.08.020

Zocchi D, Wennemuth G, Oka Y. 2017. The cellular mechanism for water detection in the mammalian taste system. *Nat Neurosci* **20**:927–933. doi:10.1038/nn.4575

Resource availability

This study did not generate new unique reagents. All materials are commercially available.

Data and code required to replicate the results reported in this paper are available from the lead contact, Ranier Gutierrez (ranier@cinvestav.mx), upon request.

Acknowledgments

We thank Mario Gil Moreno for building multielectrode arrays and Ricardo Gaxiola, Victor Manuel García Gomez, and Fabiola Hernández Olvera for their invaluable animal care. We also want to especially thank Francisco Zepeda Arias and Silvia Mejía Ortiz for their invaluable help training the subjects.

Funding

This work was supported by Productos Medix 3247, Cátedra Marcos Moshinsky, fundación Miguel Aleman Valdes, CONACyT Fronteras de la Ciencia CF-2023-G-518 (R.G.). CONACyT postdoctoral fellowship CV No.: 164310 (G.M.).

Author contributions

E.F. and RG. conceived the project. E.F. conducted experiments and performed data curation. G.M. performed code implementation and formal analysis. R.G. supervised the project and provided resources. R.G. and H.M. supervised the analysis. All authors discussed the results. G.M. wrote the original draft. All authors reviewed, edited, and approved the final manuscript.

Declaration of interests

The authors declare no competing interests.

Figures

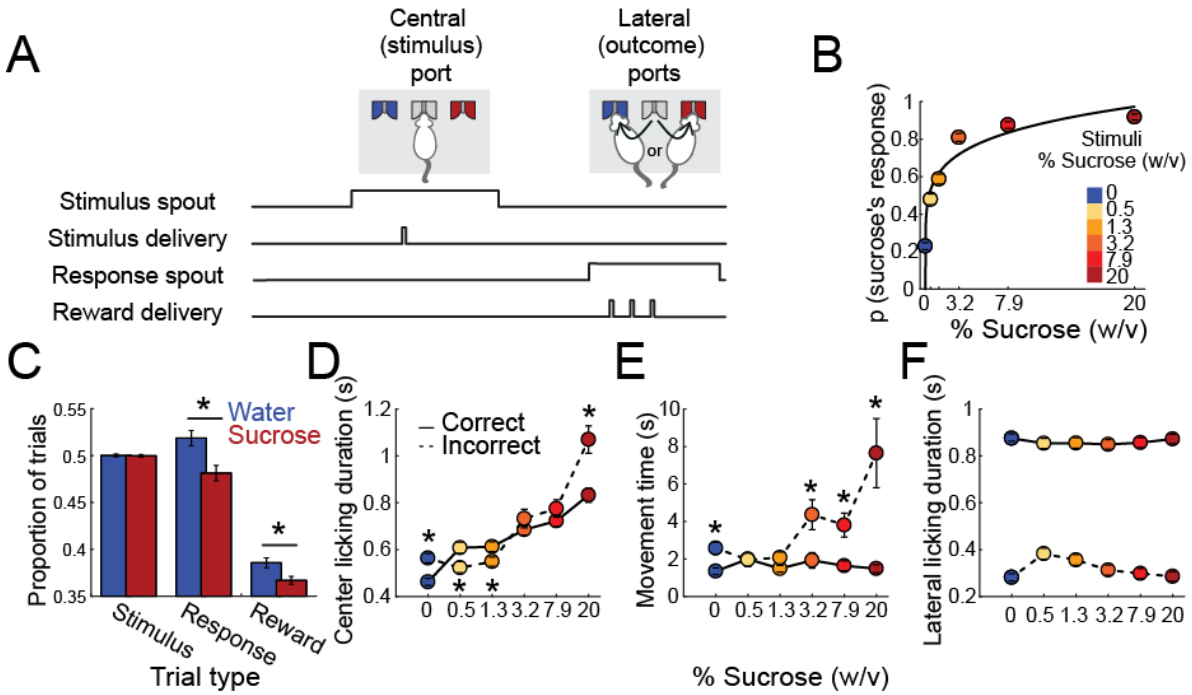

Figure 1. Water-sucrose categorization task in rats. (**A**) Schematic diagram of the behavioral setup. The rat is presented with three licking spouts: a central spout (Stimulus port) and two lateral spouts (Outcome ports). At the beginning of each trial, the rat licks the stimulus spout to receive a 10 μL drop of liquid as a stimulus. The stimulus is one of six different sucrose concentrations dissolved in water: 0 (water), 0.5, 1.3, 3.2, 7.9, and 20% w/v. The rat must then make a water/sucrose decision by licking the water- or sucrose-associated lateral spout. If the correct lateral spout is chosen, the rat receives three drops of water as a reward after one empty lick. The session is composed of 50% of water trials. The other sucrose concentrations were equally distributed over the remaining trials. (**B**) Probability of selecting the sucrose-associated lateral spout ('Sucrose' response) for each of the stimuli. The black line depicts the power fitting (R^2 = 0.87). Each stimulus is represented according to the color code displayed on the right sidebar. (**C**) Trials distribution. The proportion of trials with water (blue) or sucrose (red) is shown in the left panel. The proportion of trials in which the rat chose the water (blue) or sucrose spout (red) is shown in the

middle panel. The proportion of trials in which the rat chose the correct spout and was rewarded with water (blue) or sucrose (red) is depicted in the right panel. (**D**) Time spent licking the central spout, from stimulus delivery until the last lick, before responding to a lateral spout. The color code in panel **B** indicates the different types of stimuli that were delivered. Continuous and dashed lines indicate correct and incorrect trials, respectively. (**E**) Latency to the lateral spout's first lick after the central spout's last lick. Same conventions as in (**D**). (**F**) Licking duration at the lateral spout. Data from each subject's sessions were included and presented as mean ± SEM.

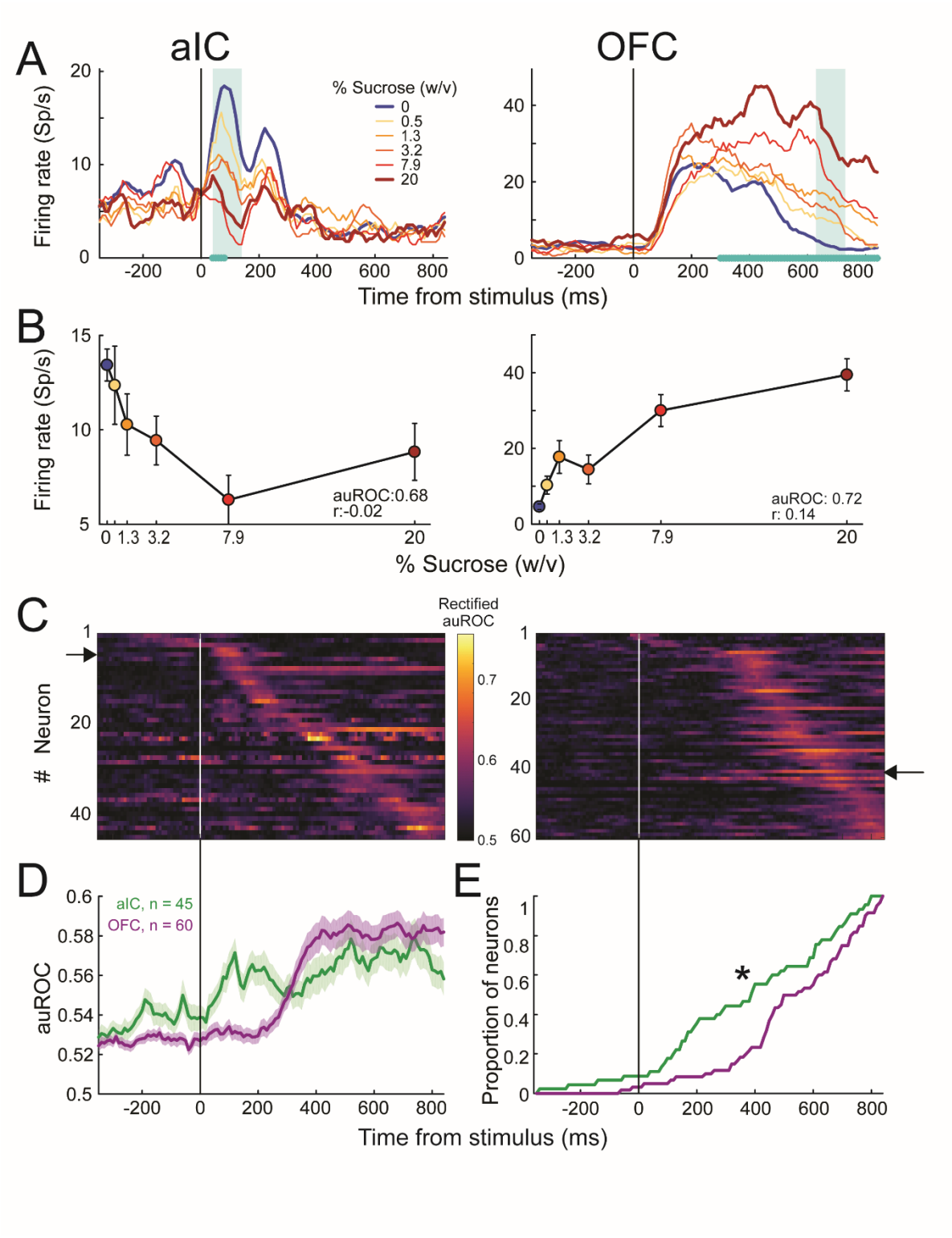

Figure 2. aIC and OFC neurons encode the presence or absence of sucrose.

(**A**) Representative examples of aIC (left) and OFC (right) neurons that respond differentially to the absence (water) and presence (scale of reds) of sucrose. The

activity is aligned (time = 0 s) with sucrose delivery in the central spout. The color code shows sucrose concentration in the upper right corner. The cyan rectangle on the abscissa indicates the best time windows (time bins with the maximum significant area under the receiver operating characteristic curve [auROC] values) for encoding stimulus information. **Figure 2 Supplementary 1** shows the proportion of recruited neurons per task epoch.

(**B**) Averaged neuronal activity during the best Stimulus-encoding time window (cyan rectangle in **A**) as a function of sucrose concentration.

(**C**) Subpopulations of aIC (left) and OFC (right panel) neurons that encode sucrose detection. The color map shows the auROC values (color code on the right) for each significant Stimulus-encoding neuron (y-axis) across time aligned to Stimulus delivery (x-axis). auROC values are depicted according to the color code on the right. Neurons are ordered according to the time of maximum auROC value. Black arrows indicate the neurons shown in (A). The stimulus was encoded in sequence for both regions, but it was slightly more sequential in aIC (SqI: 0.749; PE: 0.981; TS: 0.571) than OFC (SqI: 0.695; PE: 0.939; TS: 0.515).

(**D**) Mean auROC values per time bin for the aIC (green) and OFC (purple) subpopulations shown in (**C**).

(**E**) Cumulative proportion to time of the auROC peak values of the populations shown in (**C**). The black asterisk indicates a significant difference between distributions as determined by a two-sample Kolmogorov-Smirnov test, * $p < 0.01$. Data are presented as mean ± SEM.

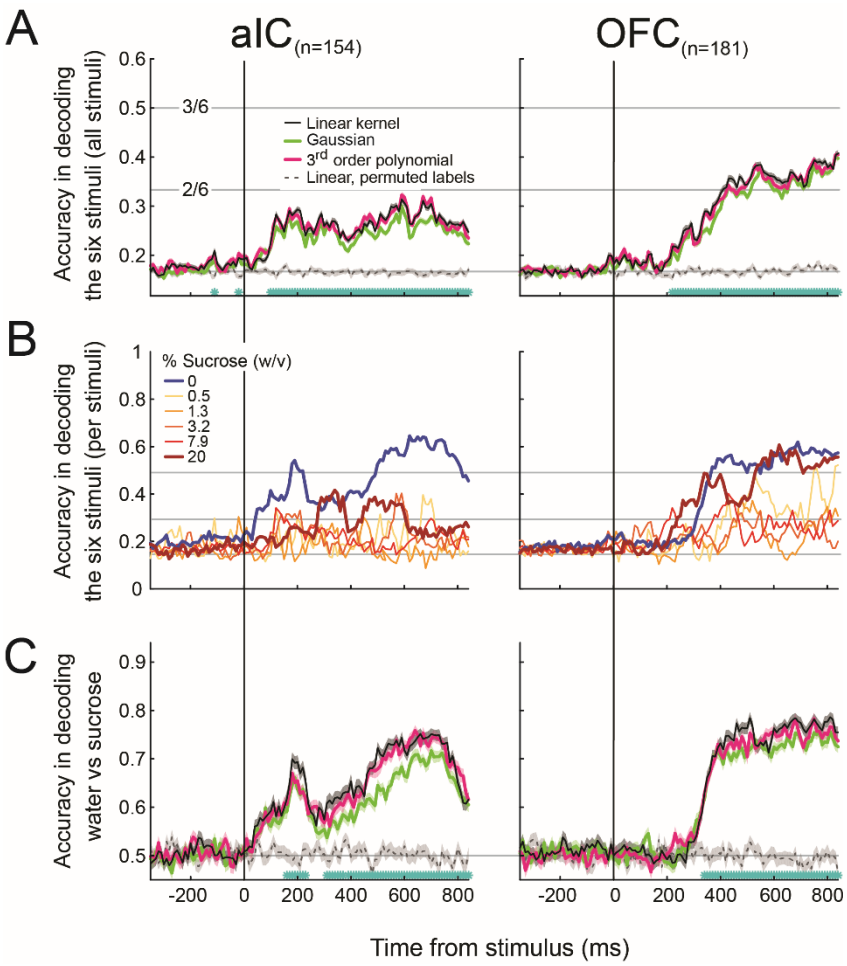

Figure 3. The qualitative distinction between water and sucrose, rather than the gradual change in intensity of the stimulus, is the most robust sensory-related information in the firing rate of the neural populations in aIC and OFC. (**A**) SVM accuracy to decode the six stimuli across time depending upon the type of kernel used. Decoders were trained with the activity of the extended population of neurons detected with ANOVA, which contains significant firing rate differences between the six stimulus concentrations and is aligned to stimulus delivery. The black, green, and pink lines depict the linear, Gaussian, and third-order polynomial kernels. The gray dashed line indicates the performance of the linear kernel after the stimulus labels have been randomly permuted. The horizontal light-gray continuous lines indicate the decoding performance for correctly identifying 1 out of 6 stimuli (chance), 2 out of 6 stimuli, and 3 out of 6 stimuli, from bottom to top. Cyan asterisks indicate bins where significant differences between the linear SVM and the linear permuted SVM were found (one-tailed t-test, $p<0.0001$, Bonferroni corrected). Data is presented as mean ± SEM.

(B) The proportion of correct classifications for each stimulus by the linear-kernel SVM is shown in (**A**).

(C) Decoding accuracy of SVMs using a linear, Gaussian, or third-order polynomial kernel to decode the water or sucrose stimulus from the activity of aIC (left) and OFC (right) neurons. The light-gray horizontal line indicates chance performance (0.5). Same conventions as in (**A**). See **Figure 3 supplementary 1**, which shows the same analysis on only the significant auROC neurons.

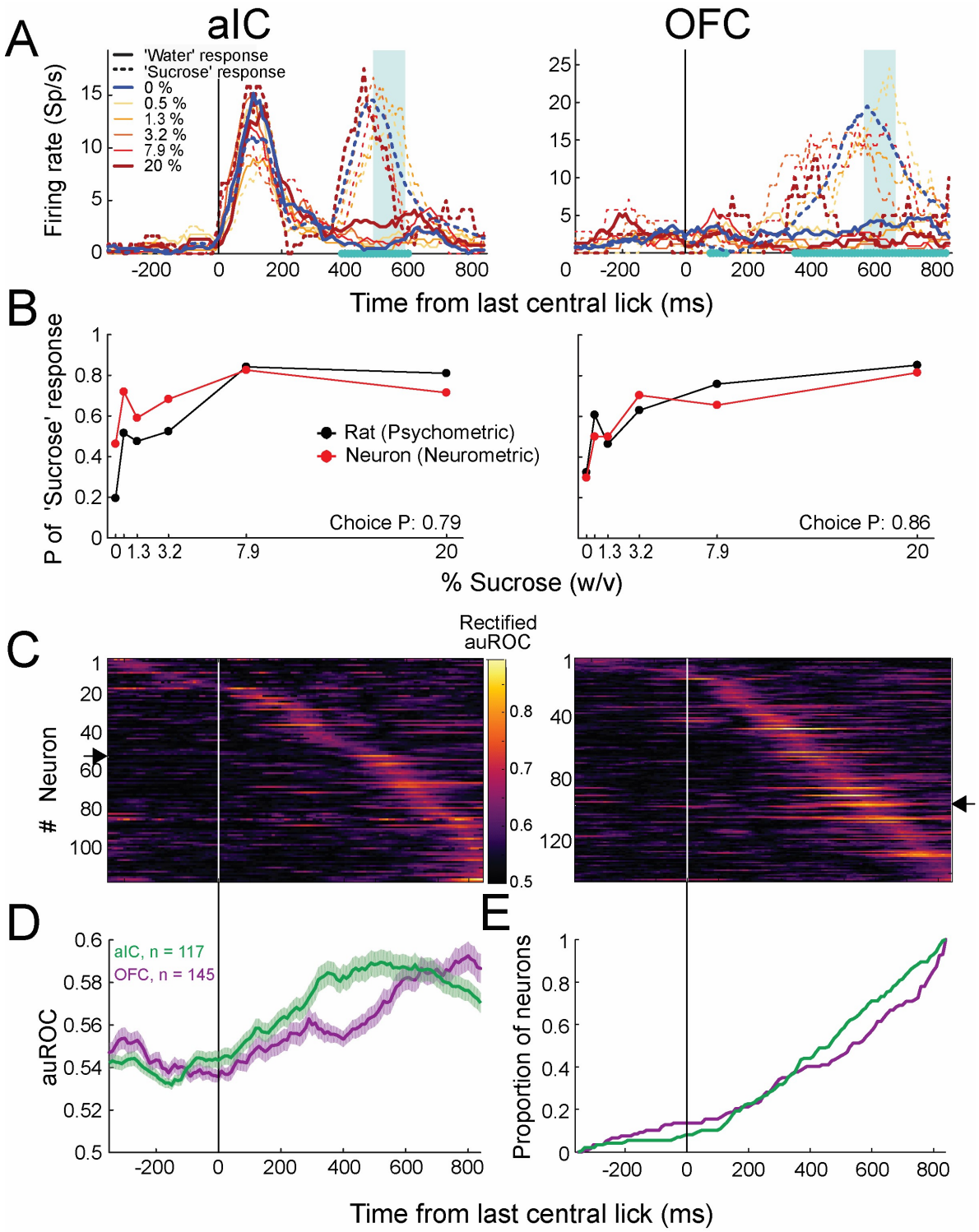

Figure 4. aIC and OFC neurons encode the categorical choice of the rats. (A) The mean firing rate of one aIC (left) and one OFC (right) neuron is selective to the animal's choice. The activity is aligned (Time = 0s) to the last lick in the central spout, encompassing the Response epoch of the trial. Neural activity is separated by stimulus (color-coded) and choice: water or sucrose choice is marked by continuous

and dashed lines, respectively. The aIC neuron exhibited a peak of activity around 400 to 600 ms only for the sucrose-response trials (dashed lines). The OFC neuron at the right panel also responded more to trials where the rat chose the sucrose response port. **(B)** Probabilities of 'Sucrose' response, obtained from the subject (psychometric; black) and predicted by the neuron (neurometric; red) as a function of the stimuli. The probabilities were calculated from the number of Sucrose-response trials in the experimental session where neurons plotted in **A** were recorded. Decoded probabilities were calculated from the activity periods cyan shaded in (**A**) by classifying each trial as water or sucrose response according to an optimum firing rate threshold (see main text). **(C)** Rectified Choice Probability values per time bin of each neuron of the Choice-encoding subpopulation of aIC (left) and OFC (right). Data aligned (Time = 0s) to last central empty lick. **(D)** Average Choice Probability values of all Choice-encoding neurons. **(E)** Cumulative proportion of Choice-encoding cells that reached their peak auROC values across time bins. The same conventions as in **Figure 2.** Data presented as mean ± SEM. See **Figure 4 Supplementary 1** for the average activity of neurons responding more to water and sucrose choices or responding to different choices at different time bins.

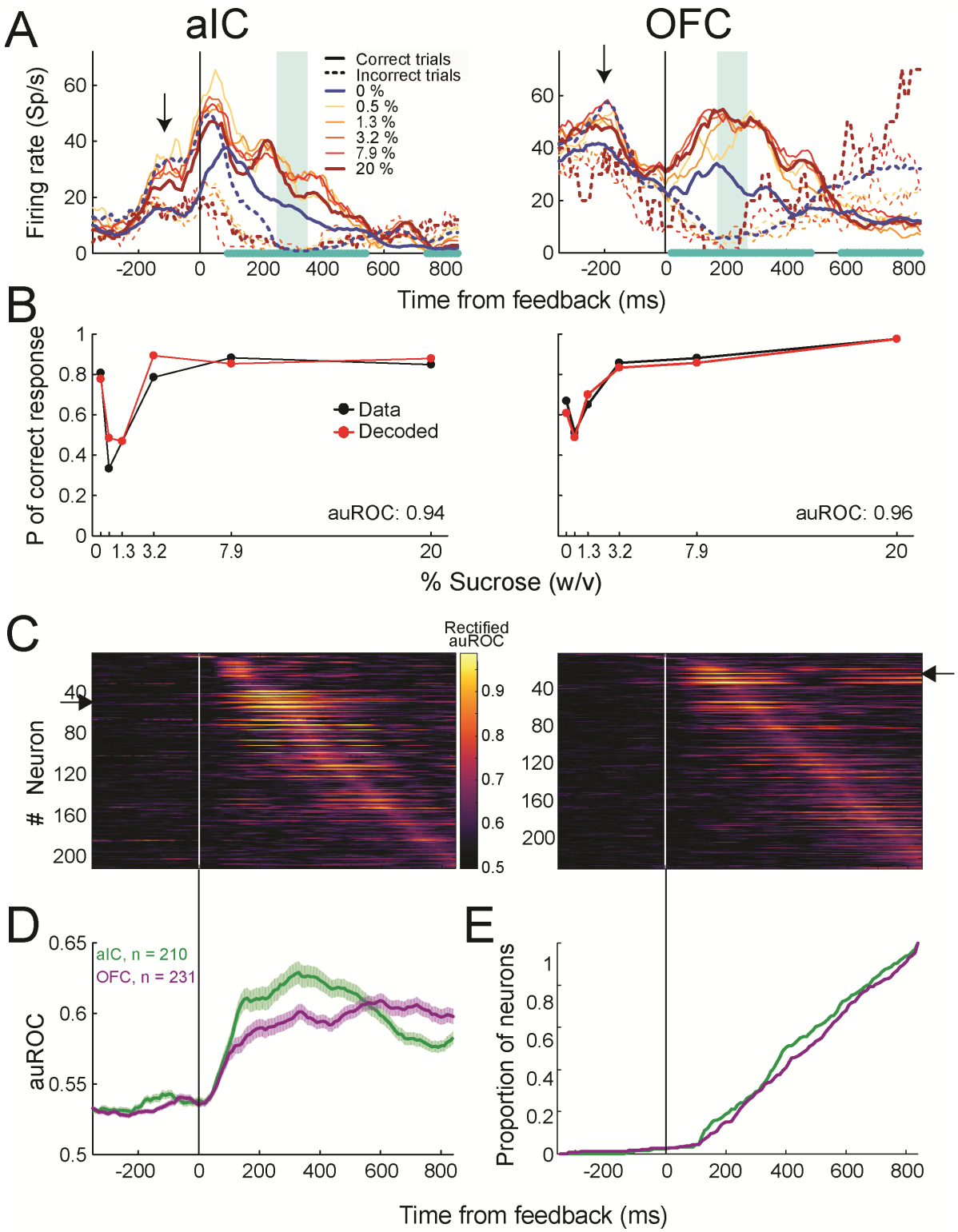

Figure 5. Neurons in aIC and OFC rapidly encode the outcome of the categorical decision. (A) The mean firing rate of one aIC (left) and one OFC (right) neuron is selective to the reward outcomes. Red asterisks on the abscissa indicate bins of significant encoding. The activity is aligned to the feedback time and

segregated by stimulus condition and outcome (see inset). **(B)** Actual and decoded probabilities of correct response as a function of the stimuli for the aIC (left) and OFC (right) neurons are shown in a). Actual probabilities were calculated from the number of correct trials in the experimental session where neurons in a) were recorded. Decoded probabilities were calculated from the activity periods shaded in gray in the panels of a) by classifying each trial as correct or incorrect, whether the neural activity surpassed the FR threshold that maximized the number of correctly classified trials (see methods). **(C)** auROC values per time bin of the population of aIC (left) and OFC (right) neurons significantly encode the outcome. Neurons were ordered according to the time of maximum auROC value. Red arrows indicate the position of the neurons depicted in a). **(D)** Mean (± SEM) across time of the auROC values of the neural populations shown in **(C)**. **(E)** Cumulative proportion of neurons from the populations shown in **(C)** that reached their peak auROC values across time bins. Inset shows the corresponding cumulative distributions of the times of the first lick in the lateral port. Same conventions as in **Figure 2**.

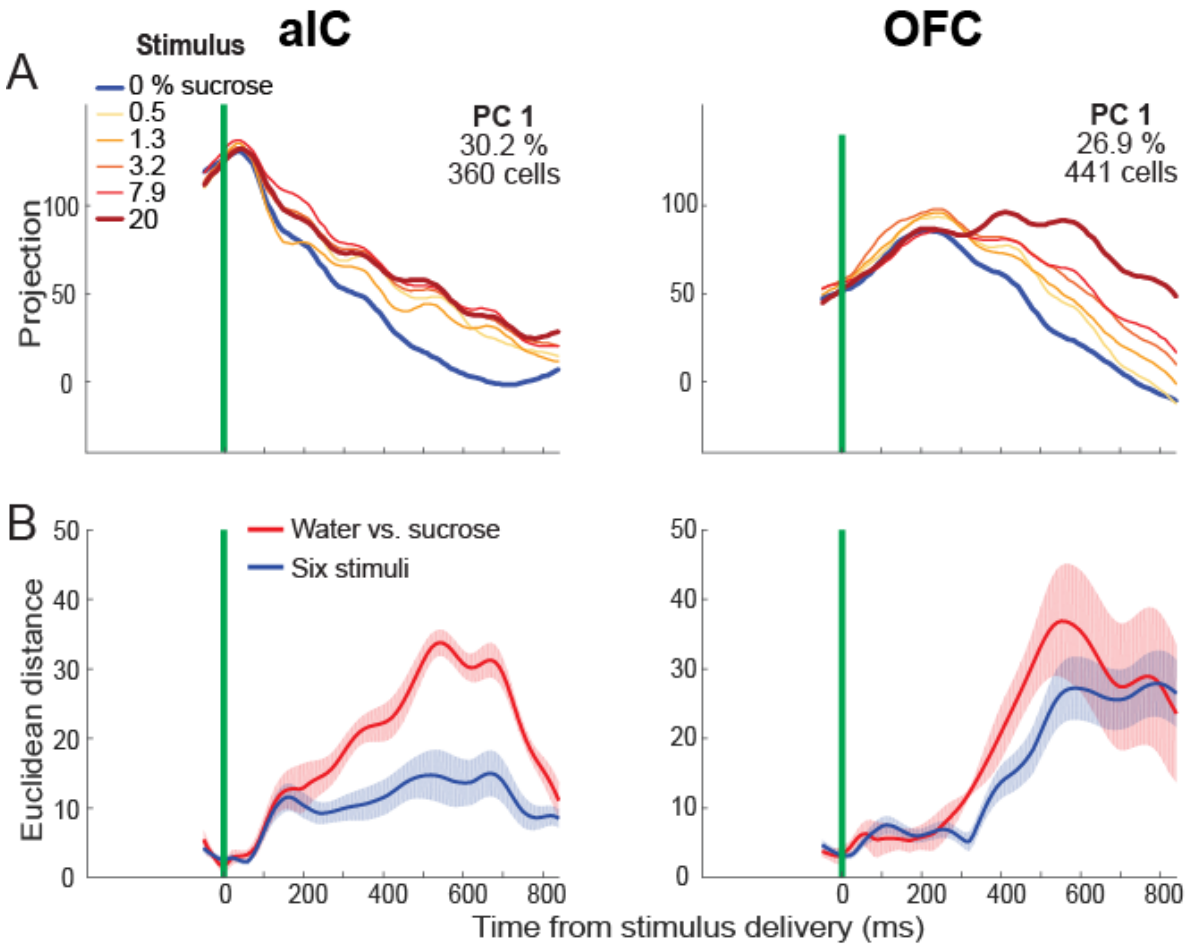

Figure 6. Principal Components reflect the difference in stimulus selectivity observed in aIC and OFC. (A) PCs calculated from the activity of aIC (left panel)

and OFC neurons (right panel). The projections are aligned to the time of stimulus delivery (green line) and are segregated by stimulus condition (the six sucrose concentrations). **(B)** Mean (± SE) Euclidean distances computed in each time bin from the projections in A. The water vs. sucrose distances were calculated from all the possible water-sucrose condition pairs (five pairs). The six stimuli distances were calculated from all the stimuli pairs (15 pairs). Compare with the temporal dynamics of decoding accuracy in **Figures 3A and 3C**.

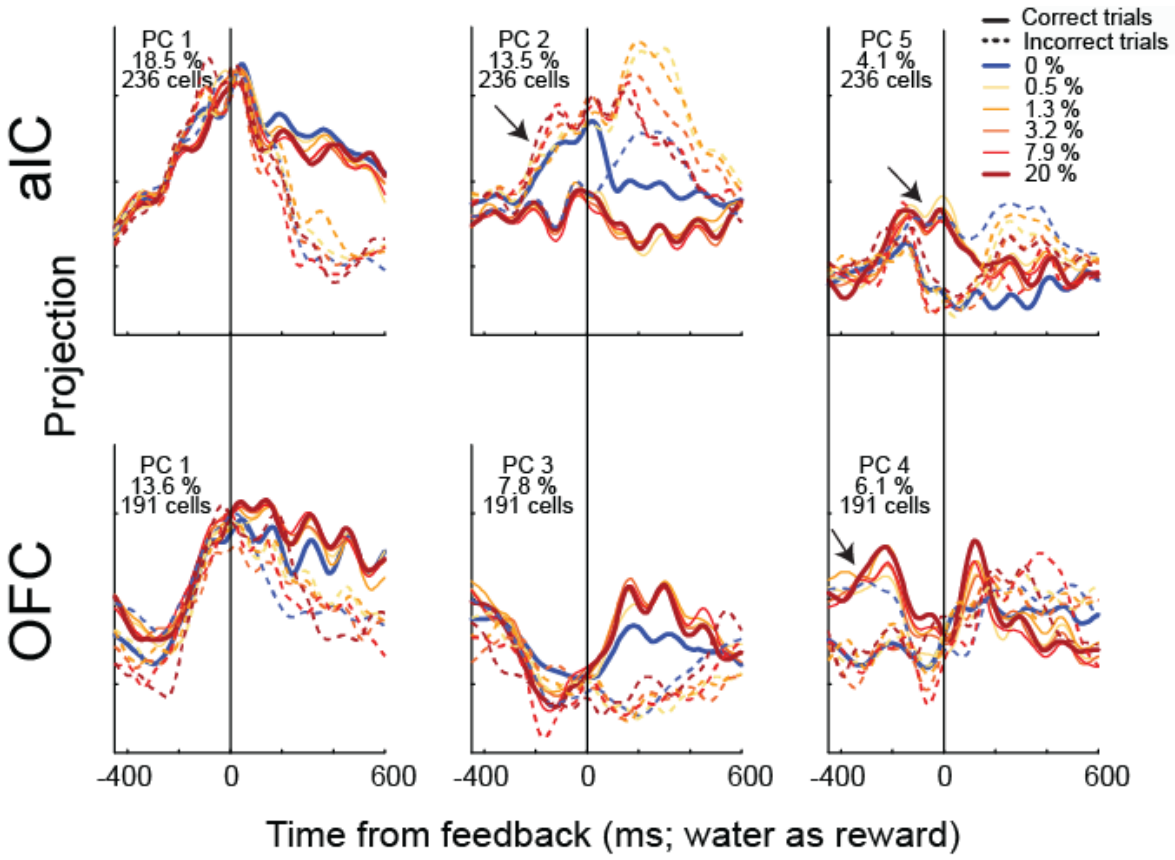

Figure 7. The main task's variables are reflected in the Principal Components of the aIC and OFC neural population activity. PCs computed with the activity of 236 aIC (upper panels) and 191 OFC (lower panels) neurons aligned to the feedback time (red line) and segregated by stimulus condition and outcome (correct or incorrect trials) as indicated in the inset in the upper right panel. Same conventions as in **Figure 6**. The arrows indicate moments when the PCA segregated information about the rat's choice. Note that OFC carries information about choice earlier than the aIC. Divergence of PCA trajectories after time 0 s indicates decoding reward outcomes.

Supplementary figures

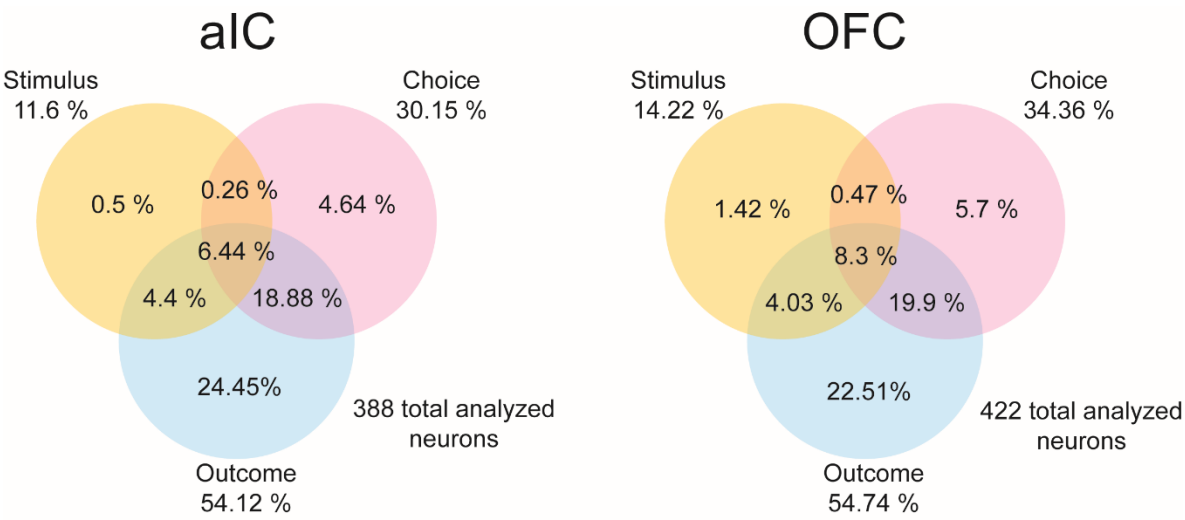

Figure 2 Supplementary 1. **Proportion of encoding neurons from the Signal Detection Theory analysis.** Numbers indicate the percentage of neurons with significant encoding related to the total number of neurons analyzed for each task variable in aIC (left panel) or OFC (right panel). Cells coding more than one parameter are indicated in the overlapped areas.

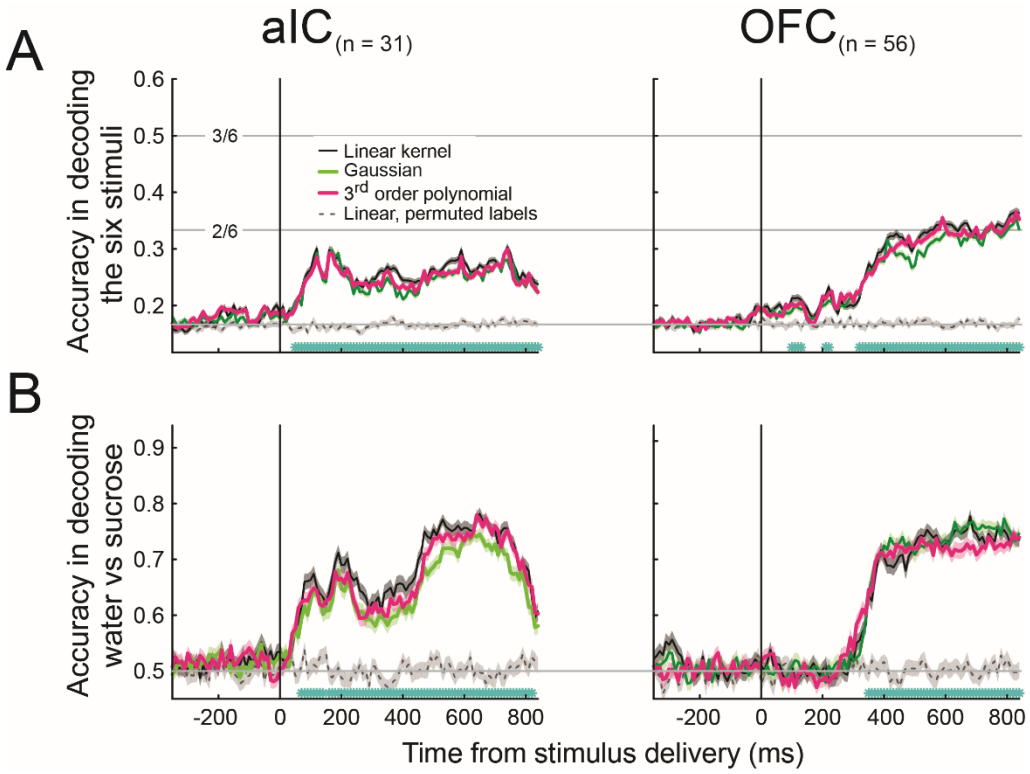

Figure 3 Supplementary 1. The distinction between water and sucrose, not the identity of the six stimuli, is the strongest taste information encoded in the firing rate of the neural populations in aIC and OFC. (A) Mean ± SEM accuracy from a linear, Gaussian, or third-order polynomial-kernel SVM trained to decode the six different stimuli (0, 0.5, 1.3, 3.2, 7.9, and 20 % sucrose) from the activity of aIC (left panel) and OFC (right panel) neurons. The gray dashed lines show the decoding accuracy from a linear-kernel SVM where the water/sucrose labels were randomly permuted. Data is aligned with the time of stimulus delivery. Cyan asterisks indicate bins where significant differences between the linear SVM and the linear permuted SVM were found (One tail, t-test, $p <= 0.0001$, Bonferroni corrected). The light gray horizontal lines indicate the decoding performance at 1/6 (chance), 2/6, and 3/6. **(B)** Accuracy from SVM trained to decode the delivery of a water (0 % sucrose) or sucrose (0.5, 1.3, 3.2, 7.9, and 20 % sucrose) stimulus from the activity of the same neurons in panel **A**). The light-gray horizontal line indicates the decoding performance at the chance (0.5). The ordinate axes in **A**) and **B**) show distinct ranges but are at the same scale. Same conventions as in panel A.

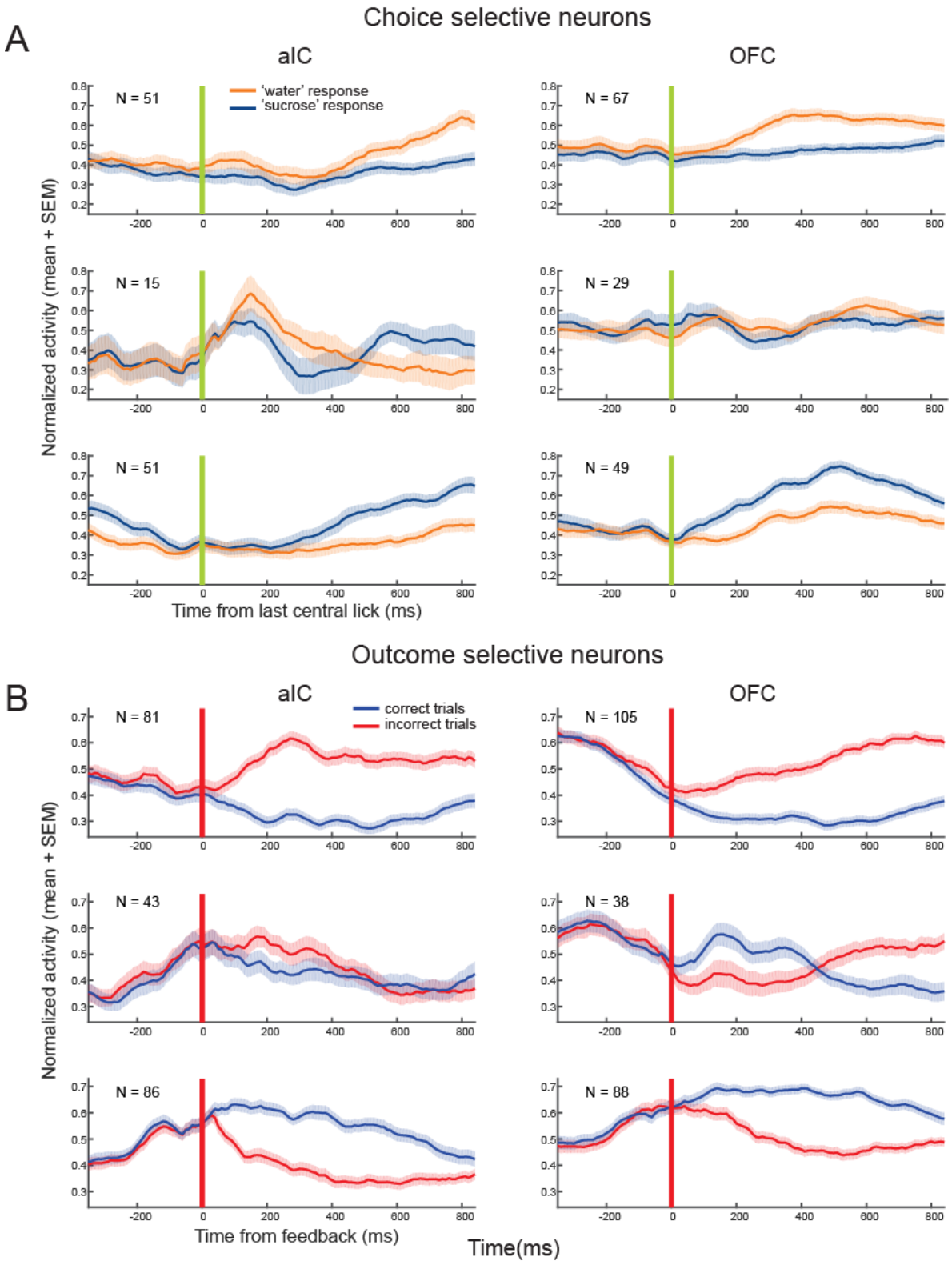

Figure 4 Supplementary 1. Neurons with higher activity for one or another decision encoding. Normalized population activity (mean ± SEM) of neurons in AIC

and OFC is selective for the rat's choice or the trial's outcome. **(A)** Green and red vertical lines indicate the time of the last lick in the central port and feedback time, respectively. Neurons encoding the choice were additionally segregated into neurons with higher activity for 'water' responses (upper panel), neurons with higher activity for 'sucrose' responses (lower panel), or neurons with changes in selectivity (intermediate panel). **(B)** Analogous segregation was performed on neurons encoding the trial's outcome. The number of neurons in each sub-population is indicated in the graphs.

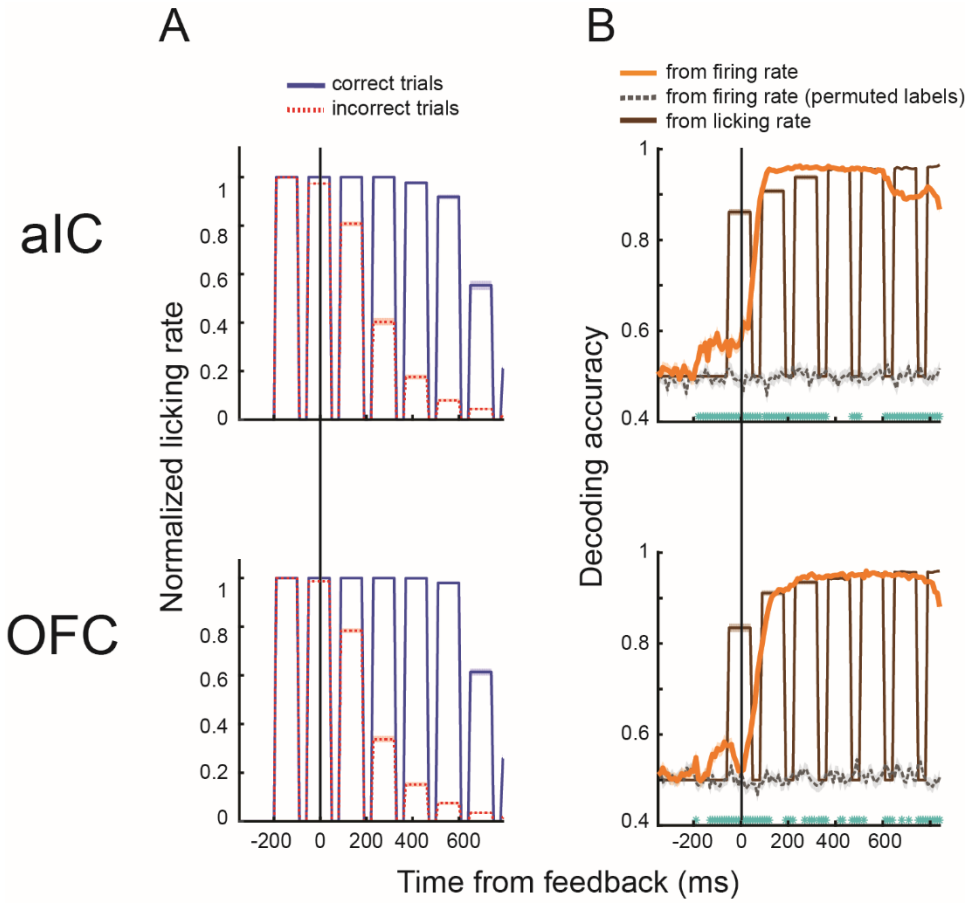

Figure 5 Supplementary 1. The rat's licking behavior does not entirely explain the encoding properties of the outcome-related neurons.

(**A**) Normalized licking rates (mean + SEM) in rewarded (blue line) and unrewarded trials (red line) from the sessions where aIC (upper panel) or OFC outcome-encoding neurons shown in **Figure 5C** were recorded.

(**B**) Accuracy in decoding rewarded from unrewarded trials (mean + SEM) using either the lick rates of the rats (brown) or the firing rates (orange) of the aIC (upper panel) and OFC neurons (lower panel) shown in the **Figure 5C**. Cyan asterisks mark the bins where the classification accuracy calculated from the firing rate differs from

that calculated from lick rates according to a bootstrapping test on the mean differences (see Methods). Note that the licking-related decoding accuracy drops to chance (0.5) periodically, but the decoding accuracy of the neural activity remains high during the post-feedback period.

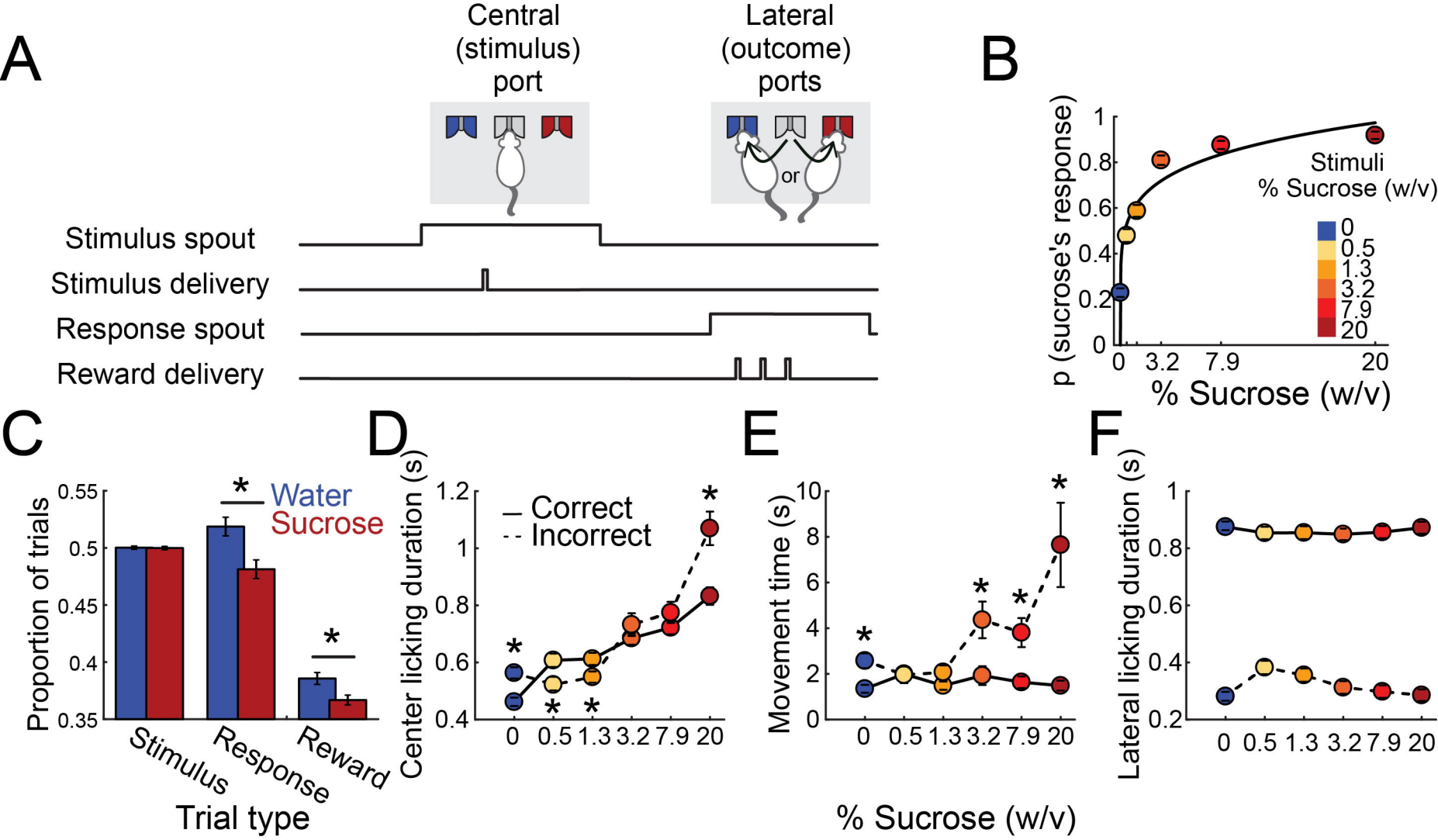
A
Central (stimulus) port
Lateral (outcome) ports
or
Stimulus spout
Stimulus delivery
Response spout
Reward delivery
B
p (sucrose's response)
% Sucrose (w/v)
Stimuli
% Sucrose (w/v)
0
0.5
1.3
3.2
7.9
20
C
Proportion of trials
Water
Sucrose
Stimulus
Response
Reward
Trial type
D
Center licking duration (s)
Correct
Incorrect
E
Movement time (s)
% Sucrose (w/v)
F
Lateral licking duration (s)

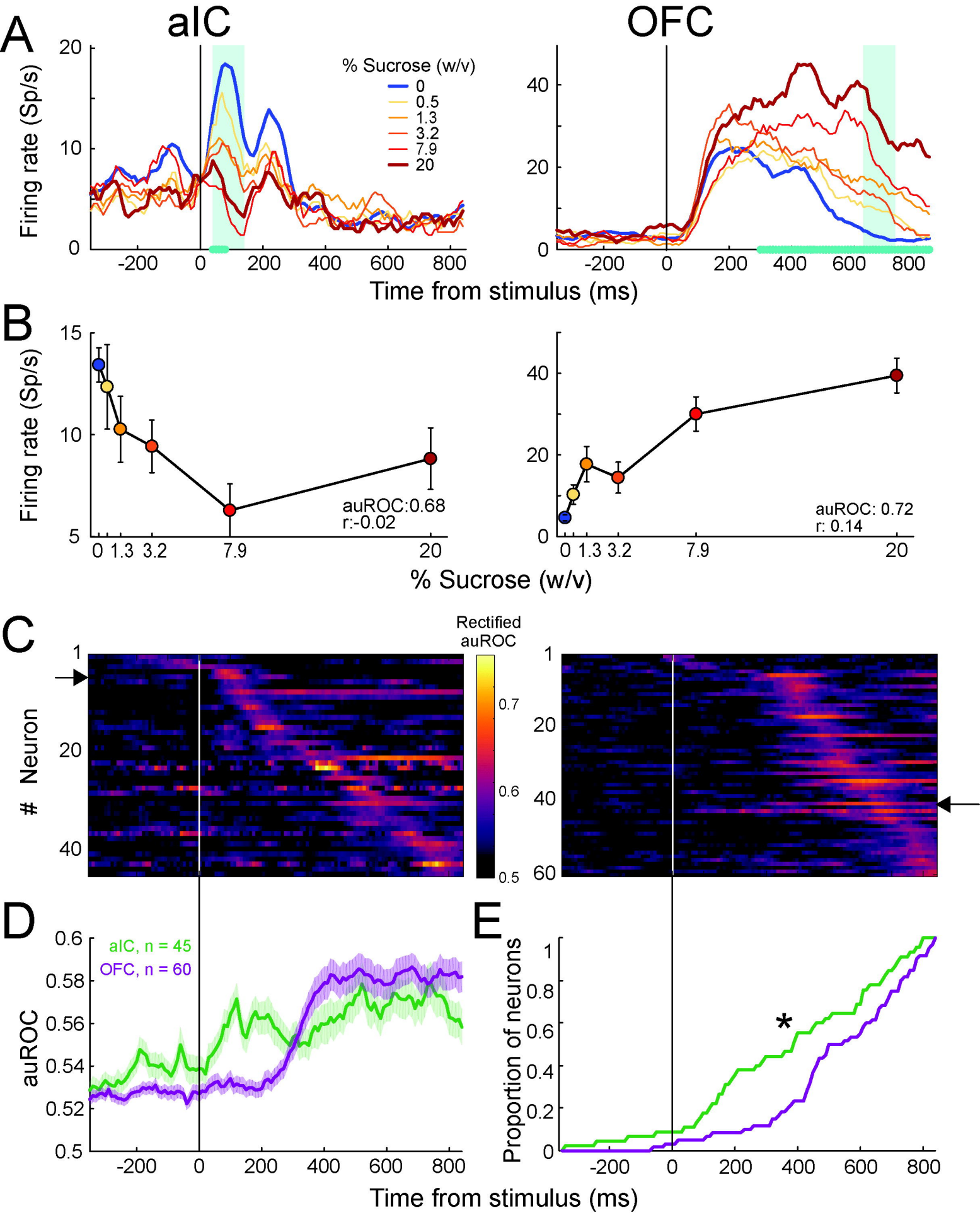
A
aIC
OFC
% Sucrose (w/v)
0
0.5
1.3
3.2
7.9
20
Firing rate (Sp/s)
Time from stimulus (ms)
B
Firing rate (Sp/s)
auROC:0.68
r:-0.02
auROC: 0.72
r: 0.14
% Sucrose (w/v)
C
Rectified auROC
Neuron
D
aIC, n = 45
OFC, n = 60
auROC
Time from stimulus (ms)
E
Proportion of neurons
*

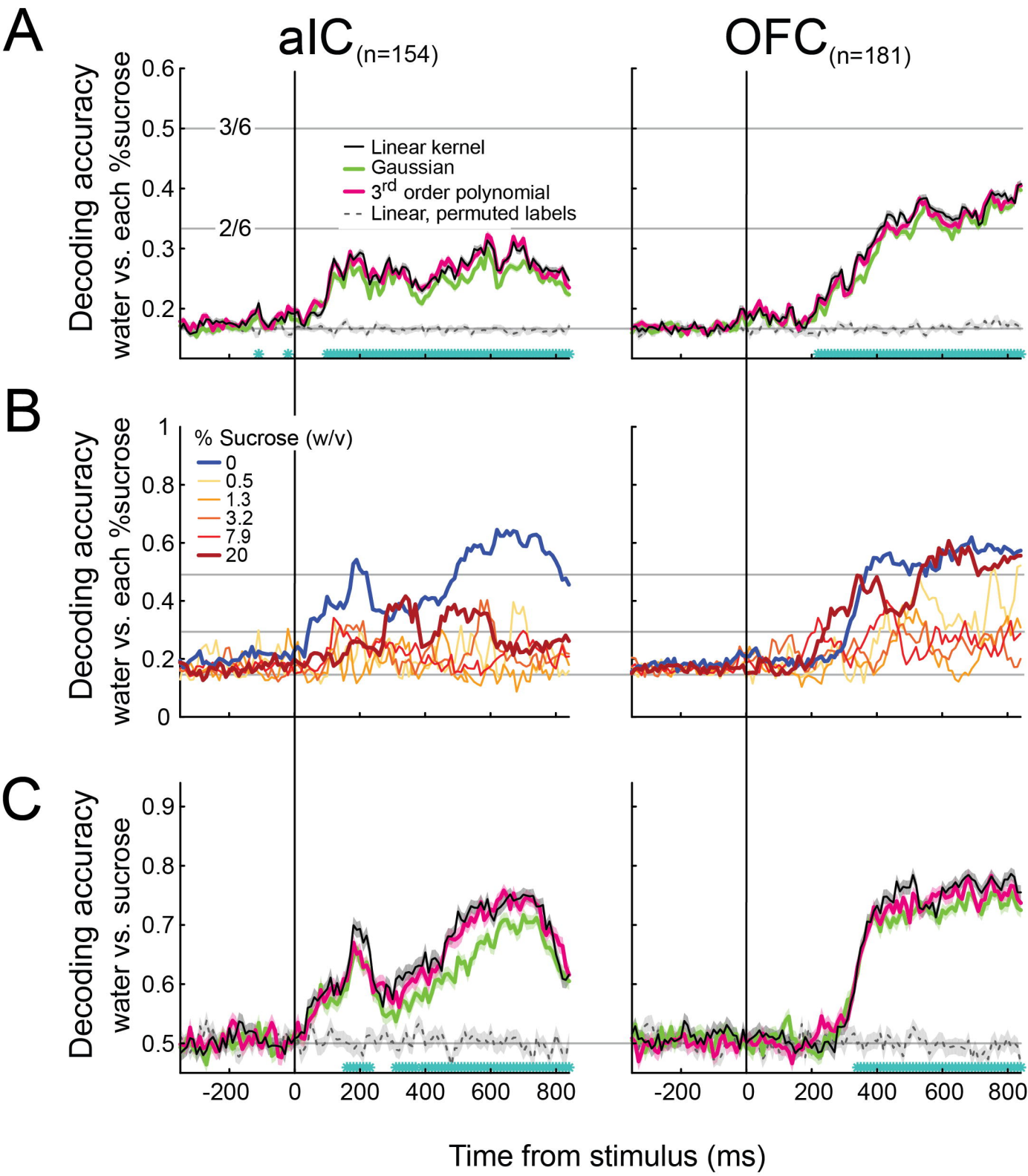
A
aIC(n=154)
OFC(n=181)
Decoding accuracy
water vs. each %sucrose
0.6
0.5
0.4
0.3
0.2
3/6
2/6
Linear kernel
Gaussian
3rd order polynomial
Linear, permuted labels
B
Decoding accuracy
water vs. each %sucrose
1
0.8
0.6
0.4
0.2
0
% Sucrose (w/v)
0
0.5
1.3
3.2
7.9
20
C
Decoding accuracy
water vs. sucrose
0.9
0.8
0.7
0.6
0.5
-200
0
200
400
600
800
Time from stimulus (ms)

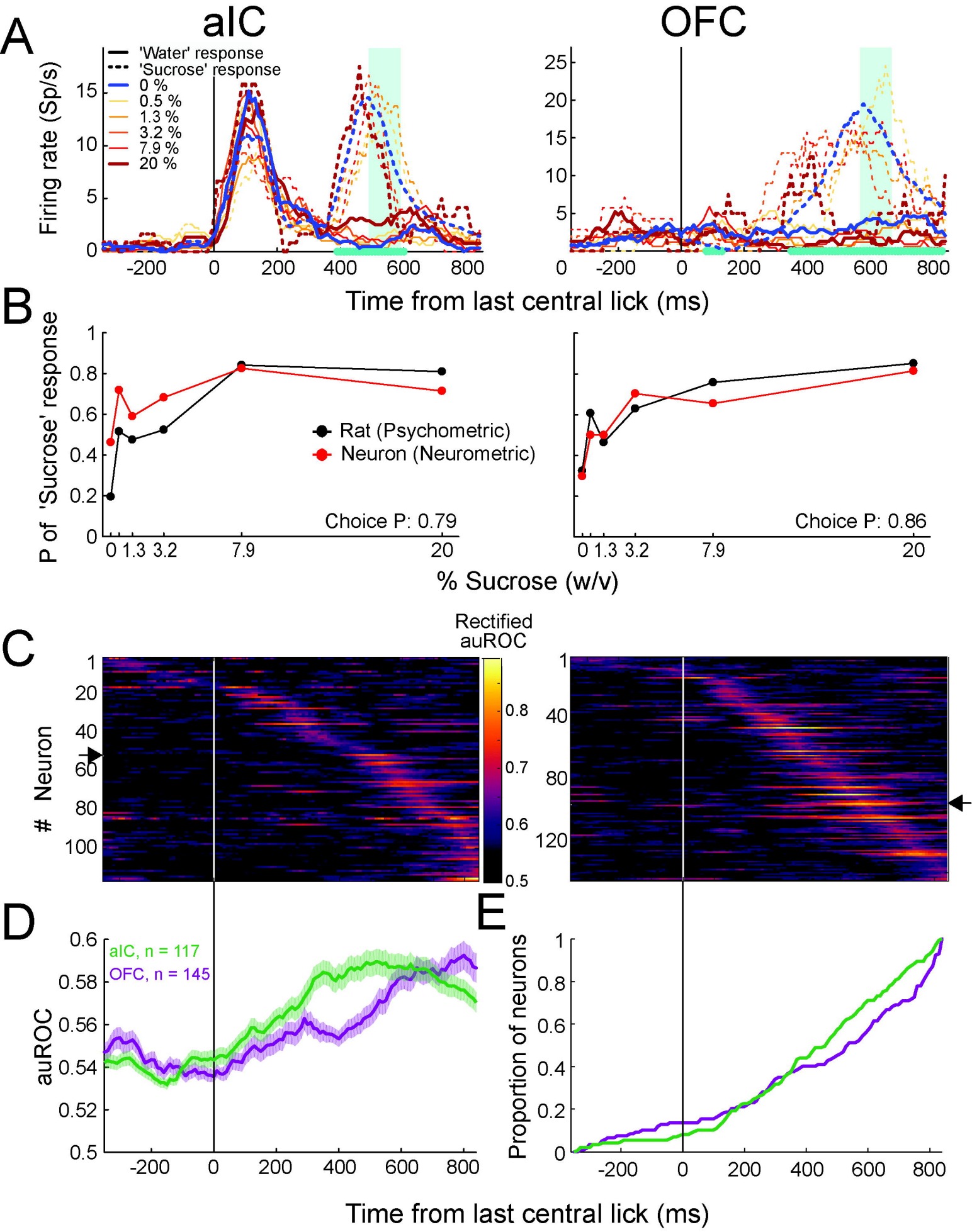
A
aIC
OFC
'Water' response
'Sucrose' response
0 %
0.5 %
1.3 %
3.2 %
7.9 %
20 %
Firing rate (Sp/s)
Time from last central lick (ms)
B
P of 'Sucrose' response
Rat (Psychometric)
Neuron (Neurometric)
Choice P: 0.79
Choice P: 0.86
% Sucrose (w/v)
C
Rectified auROC
Neuron
D
aIC, n = 117
OFC, n = 145
auROC
E
Proportion of neurons
Time from last central lick (ms)

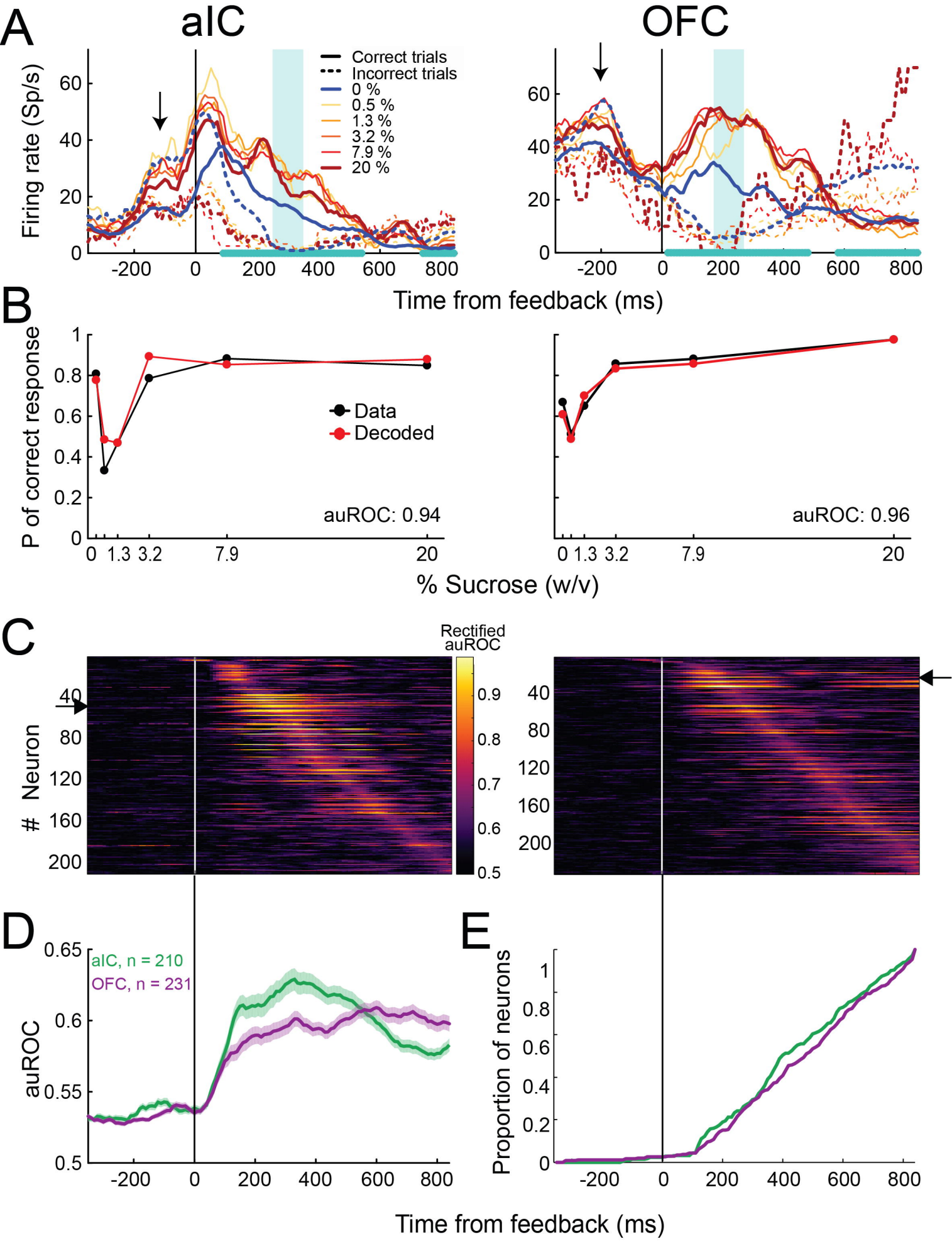
A
aIC
OFC
Correct trials
Incorrect trials
0 %
0.5 %
1.3 %
3.2 %
7.9 %
20 %
Firing rate (Sp/s)
Time from feedback (ms)
B
P of correct response
Data
Decoded
auROC: 0.94
auROC: 0.96
% Sucrose (w/v)
C
Rectified auROC
Neuron
D
aIC, n = 210
OFC, n = 231
auROC
E
Proportion of neurons
Time from feedback (ms)

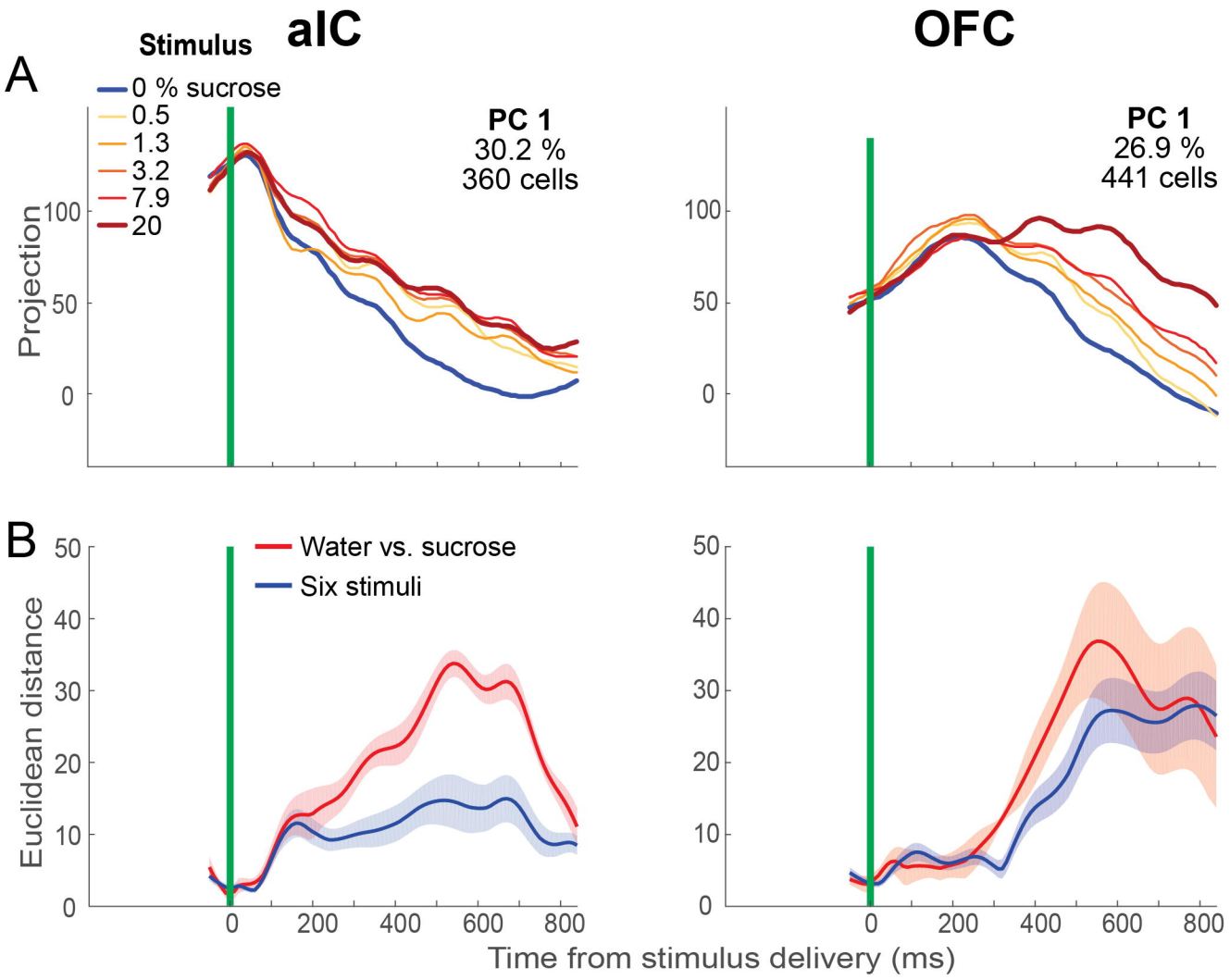
aIC
OFC
A
Stimulus
0 % sucrose
0.5
1.3
3.2
7.9
20
PC 1
30.2 %
360 cells
PC 1
26.9 %
441 cells
Projection
100
50
0
B
Water vs. sucrose
Six stimuli
Euclidean distance
50
40
30
20
10
0
0
200
400
600
800
Time from stimulus delivery (ms)

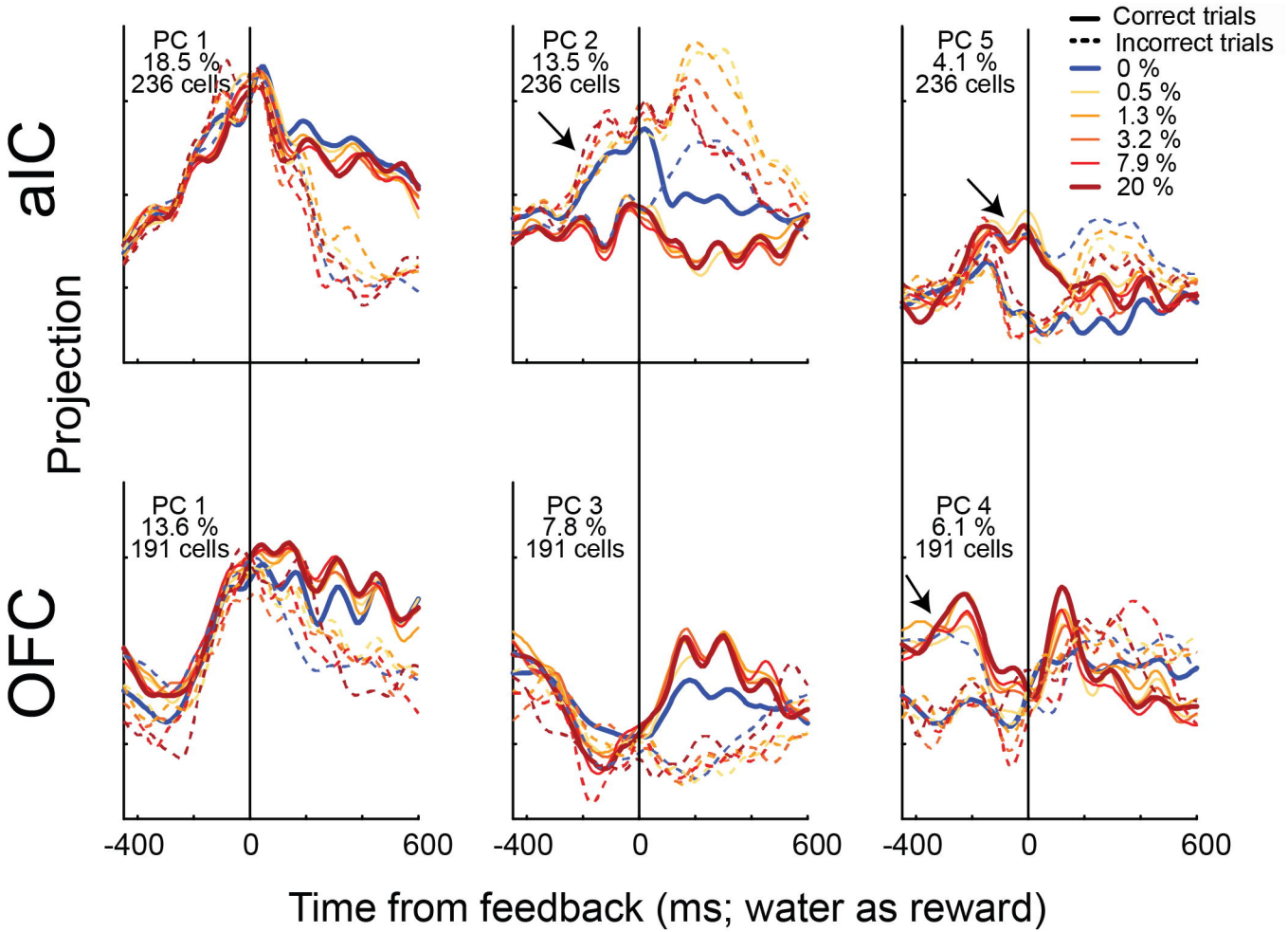
aIC
OFC
Projection
PC 1
18.5 %
236 cells
PC 2
13.5 %
236 cells
PC 5
4.1 %
236 cells
PC 1
13.6 %
191 cells
PC 3
7.8 %
191 cells
PC 4
6.1 %
191 cells
Correct trials
Incorrect trials
0 %
0.5 %
1.3 %
3.2 %
7.9 %
20 %
-400
0
600
Time from feedback (ms; water as reward)